ISTANBUL TECHNICAL UNIVERSITY ★ GRADUATE SCHOOL OF SCIENCE ENGINEERING AND TECHNOLOGY

SIMULATION OF CONTINOUS POLYSTYRENE PARTICLE MANIPULATION WITH DIELECTROPHORESIS USING COMSOL

M.Sc. THESIS

Yavuz GENÇ

Department of Nanoscience&Nanoengineering

Nanoscience&Nanoengineering Programme

MAY 2015

ISTANBUL TECHNICAL UNIVERSITY ★ GRADUATE SCHOOL OF SCIENCE ENGINEERING AND TECHNOLOGY

SIMULATION OF CONTINOUS POLYSTYRENE PARTICLE MANIPULATION WITH DIELECTROPHORESIS USING COMSOL

M.Sc. THESIS

Yavuz GENÇ
(513111015)

Department of Nanoscience&Nanoengineering

Nanoscience&Nanoengineering Programme

Thesis Advisor: Prof. Levent TRABZON

MAY 2015

İSTANBUL TEKNİK ÜNİVERSİTESİ ★ FEN BİLİMLERİ ENSTİTÜSÜ

ALTERNATİF AKIM KUTUPSAL DEVİNİM İLE SÜREKLİ AKIŞTA POLİSTREN PARÇACIKLARIN YÖNLENDİRİLMESİNİN COMSOL SİMULASYONU

YÜKSEK LİSANS TEZİ

Yavuz GENÇ
(513111015)

Nanobilim & Nanomühendislik Anabilim Dalı

Nanobilim & Nanomühendislik Programı

Tez Danışmanı: Prof. Dr. Levent TRABZON

MAYIS 2015

Yavuz Genç, a **M.Sc.** student of ITU **Graduate School of Science Engineering and Technology** student ID **513111015**, successfully defended the **thesis** entitled "**Polystyrene Particle Manipulatıng Using AC Dielectrophoresis**", which he prepared after fulfilling the requirements specified in the associated legislations, before the jury whose signatures are below.

Thesis Advisor :	**Prof. Dr. Levent TRABZON** İstanbul Technical University	....
Jury Members :	**Doç. Dr. Esra Özkan Zayim** İstanbul Technical University	....
	Yrd. Doç. Dr. Melikhan Tanyeri İstanbul Şehir University	....

Date of Submission : 21 April 2015
Date of Defense : 12 May 2015

FOREWORD

I would like to express my sincere thanks, gratitude and regards to my advisor Professor Levent Trabzon for his patience, guidance and advices. I am grateful for that experience and I consider myself lucky to have him as my advisor. I would like to thank Professor Ali Beşkök and Professor Hüseyin Kızıl for their advices and support.

I would like to acknowledge my co-worker Emre Altınağaç, without him I would not be where I am today with my research. To all the members of the ITU MEMs research group (past and present) thanks for making the place fun. A special thanks to Mümin Balaban and Muhammed Bekin for being there as long as I am and for highly enjoyable lunch and coffee breaks.

In addition, many thanks to my colleague İlker Şengüzel from 3M who has guided me while using the statistical tools to optimize my study and Cihan Dizman from 3M who encourage me to finalize my thesis while I am working for him.

I would also like to take this opportunity to express my thanks to the supports obtained from my family and close friends and for their encouragements and understanding during this journey.

To my father, you will be missed and remain in my heart, even you could not see me finishing my master you have always supported me.

April 2015 Yavuz GENÇ

TABLE OF CONTENTS

Page

ABBREVIATIONS

AC	: Alternative Current
CM	: Clausius-Mossotti
DC	: Direct Current
DEP	: Dielectrophoresis
LOC	: Lab on a Chip
pDEP	: Positive Dielectrophoresis
PDMS	: Polydimethylsiloxane
nDEP	: Negative Dielectrophoresis
MEMS	: Microelectromechanical Systems
BSA	: Bovine Serum Albumin
PBS	: Phosphate Buffered Saline
DNA	: Deoxyribonucleic acid
3D	: 3 Dimensional
CAGR	: Compound Annual Growth Rate

LIST OF TABLES

LIST OF FIGURES

Page

SIMULATION OF CONTINOUS POLYSTYRENE PARTICLE MANIPULATION WITH DIELECTROPHORESIS USING COMSOL

SUMMARY

In the near feature, we will see complicated and sophisticated Lab-On-a-Chip (LOC) devices for many kinds of medical application, which will fit on ones palm and does the job of a high tech laboratory. For enhancing such kinds of devices, the physical and chemical truths, theories, phenomenon will interlace with micro & nano technology.
Dielectrophoresis (DEP) is a non-destructive, electro kinetic transport mechanism with potential for the separation and manipulation of bio particles in microfluidics devices. With the developments in the Microelectromechanical systems (MEMS) and nanotechnology, a large electric field with weak voltages can be obtained for manipulating, separating, and characterizing micro/ nano-sized particles such as cells, Deoxyribonucleic acid (DNA), proteins, nanotubes, and nanoparticles. In order to make adequate devices the design and simulation should well correlated to get most feasible and optimum geometry of the electrodes and the micro channel network.
Basics of the DEP simulations lies on proper estimation, characterization and usage of Electro hydrodynamic forces and their effects. Simulation generally involves the electrical potential field, the flow field and the particle tracing. A three Dimensional (3D) model of the DEP chip on Multiphysics software can do simulation of these physical results.
In this thesis work, angular interdigitated electrodes and Polydimethylsiloxane (PDMS) channels designed to separate the polystyrene particles and two different Comsol simulations has been performed.
In the first simulation, a basic model that has only two electrode couples is used. A statistical approach known as surface response is used to obtain an optimization model for this simple model with the results obtained from Comsol simulation. An equation is generated and optimized running conditions identified for the simple model.
In the second simulation, a realistic model, which has 43 electrode couples, is used. Same boundary conditions, initial conditions and estimations applied in both model. Electrostatic, flow and particle tracing modules used in Comsol simulations and results obtained for a parameter group.
After that, fabrication of the LOC device explained in details and experimental setup introduced. Before the experiments, Bovine Serum Albumin (BSA) solution with Phosphate Buffered Saline (PBS) is pumped and held inside the micro channel for inhibiting the fouling. The experiment performed with the same parameter group used in Comsol simulation and results shared which are similar to the simulation results. 3.2 μm particles (Red fluorescent) are separated from the 9.8 μm particles (Green fluorescent) in both simulation and experiment. This work was supported by TUBITAK under Project No. 111M730.

ALTERNATİF AKIM KUTUPSAL DEVİNİM İLE SÜREKLİ AKIŞTA POLİSTREN PARÇACIKLARIN YÖNLENDİRİLMESİNİN COMSOL SİMULASYONU

ÖZET

Yakın gelecekte karmaşık ve çok işlevli yonga üstü sistemler ile bütün medikal uygulamalar yapılabilir hale gelecektir ve bu işi yapan aletler mevcut büyük boyuttaki laboratuvarları bir insanın avcuna sığdıracaktır. Bunların mümkün olması fizik, kimya, biyoloji gibi ana alanları harmanlayan disiplinler arası mikro ve nano teknoloji çalışmaları ile olacaktır.

Yonga üstü sistemlerin pazarı git gide büyümektedir ve her geçen gün yapılan araştırmalar hem bilimin gelişmesine, hem yeni çözümlerin dünyaya sunulmasına olanak vermektedir. Bu alanda yapılan çalışmaların sayısı da her geçen gün katlanarak artmaktadır.

1950'li yıllarda ortaya atılan kutupsal devinim elektro kinetik bir taşıma mekanizmasıdır ve hızla gelişen mikro elektromekanik ve nano teknolojiden faydalanarak bu mekanizmanın yardımıyla biyolojik parçacıkların yönlendirilmesi yapılabilir. Bu yöntem ile DNA, protein, nanotüpler, nanoparçacıklar, mikro parçacıklar, canlı hücreler yönlendirilebilir, ayrıştırılabilir veya yakalanabilirler.

Alternatif Akım Kutupsal devinim asimetrik elektrik alan altında yalıtkan parçacıkların hareketidir. Uygun koşullar altında canlı parçacıklar mikro sistemler içinde kutupsal devinim ile yönlendirilebilirler. Sürekli akış altında bu parçacıkların sıvının sürüklenme kuvveti ve kutupsal devinim kuvvetinin dengelenmesiyle ayrıştırılması mümkündür.

Kutupsal devinimin yönü ve şiddeti Clausius-Mossotti etkenine (CM etkeni) bağlıdır. Bu etken uygulanan elektrik alanın frekansına, parçacık ve ortamın dielektrik sabitlerine göre pozitif ya da negatif olmaktadır. Eğer bir parçacık kendini saran ortama göre daha çok kutulanabilirse CM etkeni pozitif ve parçacık üzerine etki eden kutupsal devinim kuvveti de pozitif olmaktadır. Benzer şekilde parçacık kendini saran ortama göre daha az kutuplaşabiliyor ise CM etkeni ve parçacık üzerine etki eden kutupsal devinim kuvveti negatif olmaktadır. Pozitif kutupsal devinim etkisi altında parçacık elektrik alanın yoğun olduğu bölgelere doğru yönlenirken, negatif kutupsal

devinim etkisi altında parçacık elektrik alanın düşük yoğunlukta olduğu bölgelere doğru yönlenmektedir.

Pozitif kutupsal devinimin etkin olduğu polistiren parçacık ve saf su karışımında farklı boyuttaki parçacıklar farklı miktarlarda kutupsal devinim kuvvetine maruz kalacaktır. Bu özellik kullanılarak sıvının sürüklenme kuvvetinin sadece bir parçayı yolundan saptırmadan diğerine etki ederek mikro kanal içinde ayrıştırılması sağlanabilir.

Bahsedilen sistemin tasarımı, basit ve gerçekçi simülasyonları, istatistiksel optimizasyonu ve deneyleri bu tez kapsamında yapılan çalışmaların ana hatlarını oluşturmaktadır.

Tasarım aşamasından literatür taraması yapılmıştır ve bu tarama sonucunda birbirine geçmeli elektrotlar ile polistiren parçacıkların ayrıştırılmasının yapıldığı görülmüştür. 45 derece açılı birbirine geçmeli elektrotlar ile iki girişi ve iki çıkışı olan bir tasarım yapılarak L-EDIT ile maskeleri hazırlanmıştır. Ayrıca yine bu geometriler göz onuna alınarak sistemin basitleştirilmiş ve gerçekçi simülasyonları hazırlanmıştır.

Parçacık üzerine etkiyen kutupsal devinimin yönünü, akış nedeniyle doğan kuvvetlerin yönünü belirlemek için COMSOL Multiphysics 4.3a yazılımı ile elektrostatik ve akış çözümlemeleri yapılmıştır. Farklı akış hızlarında ve potansiyellerde uygulanan koşullara göre potansiyel değişimleri, elektrik alan şiddetleri, kutupsal devinim yönü akış profili, parçacık hareketleri bu yazılım ile incelenmiştir.

İki farklı simülasyon yapılmıştır ve bunların ilki basitleştirilmiş, sadece iki elektrot çiftinin modellenmesi ve bu modelin çözümünün bağlı olduğu akış hızı, elektrik potansiyeli ve parçacık çapının istatistiksel bir yazılım olan Minitabtaki Yanıt Yüzeyi metodu ile optimizasyonunun yapılmasında kullanılmıştır. Bu optimizasyon çalışması yüksek kapasiteli bilgisayar donanımına ihtiyaç duyduğu için ikinci model olan ve 43 adet elektrot çifti içeren daha karmaşık modelde kullanılmamıştır. İkinci modelin analiz sonuçları verilmiş ve bunun doğrulanması için yapılan deneylere geçilmiştir.

Gerçekçi olarak oluşturulan Comsol modelinin ve basitleştirilmiş modelin üzerinden, elektrik potansiyelleri 3 boyutlu olarak çizdirilmiş ve bunların değerleri grafiksel olarak gösterilmiştir. Sonrasında bu elektrik potansiyeline bağlı olarak oluşan 3 boyutlu elektrik alan çizdirilmiş ve elektrotların kanal boyunca nasıl bir elektrik alan oluşturdukları, elektrik alan kuvveti grafiksel olarak verilmiştir.

Elektrik alan simülasyonları sonrasında akış simülasyonu yapılmıştır. Burada kanal girişlerinin birinden gerçek modele uygun olarak parçacık ve saf su karışımı diğerinden sadece saf su girişi tanımlanmıştır. Oluşan akış profilleri 3 boyutlu olarak verilmiş ve bunların grafiksel olarak kanal girişi, ortası ve çıkışındaki değerleri paylaşılmıştır.

Elektrik alan ve akış simülasyonlarından elde edilen çözümler parçacık izleme modülüne tanımlanarak parçacıkların ve saf suyun kutupsal devinim özellikleri verilerek parçacık hareketleri 3 boyutlu olarak elde edilmiştir ve bunların ortalama kanal boyunca hareketleri grafiksel olarak verilmiştir. Ek olarak parçacıkların bu hareketleri sırasında maruz kaldıkları sıvının sürüklenme ve kutupsal devinim kuvvetinin etkileri gösterilmiştir ve parçacıkların nasıl ayrıştırıldığı açıklanmıştır.

Simülasyonun yapıldığı ve ayrışmanın görüldüğü parametreler (voltaj, akış hızı, parçacık çapı) belirlenerek deney ile simülasyonların doğruluğunun tespitinin yapılmasına olanak tanınmıştır.

Deneylerin yapılması için tasarımı paylaşılan yonga-üstü sistem üretilmiştir. Bu yonga-üstü sistem, cam altlık üzerinde 200 nm kalınlıkta Ti elektrot ve akışkanın bu elektrot üzerinde konumlanmasını sağlayan PDMS kanala sahiptir.

Standart fotolitografi ve fiziksel buhar biriktirme yöntemleri ile yonga tabanlı deney düzenekleri üretimi gerçekleştirilmiştir. Bu çalışmada AZ 1505 pozitif fotorezist cam altlık üzerine döner kaplama cihazı ile 400 nm kalınlıkta olacak şekilde kaplanmıştır. Cam altlıkların temizlenmesi fotorezistin yüzeye daha iyi kaplanabilmesi ve eş dağılımlı bir yüzey elde edilmesi için çok önemlidir. Cam altlıklar 1 molar KOH çözeltisinde 10 dakika ultrasonik karıştırıcı içerisinde bekletilmiş, saf su ile banyo edildikten sonra aseton dolu bir kapta ultrasonik karıştırıcı içerisinde 10 dakika bekletilmiştir. Sırasıyla alkol ve saf su ile banyo edilip kurutulmuştur. Elektron ışını ile buharlaştırma yöntemi kullanılarak Ti hedef malzemeler buharlaştırılmış ve fotorezist kaplı cam altlıklar üzerine Ti kaplaması yapılmıştır. Üzerinden akım geçen filament kopan elektronlar, manyetik saptırıcılarla Ti yüklü pota üzerine düşürülerek, hedef metalin buharlaşmasını sağlamaktadır. Fotorezist kaplı cam altlıklar üzerine 200 nm Ti kaplandıktan sonra, fotorezist aseton ile çözündürülüp yüzeyden uzaklaştırılmış ve istenilen tasarımlarda elektrotlar cam yüzey üzerinde elde edilmiştir.

Sonrasında ayrıştırılmak istenen parçacıklar ve saf su çözeltisini elektrotlar üzerinde geçirebilmek için gereken PDMS kanal üretilmiştir. PDMS, sıvı haldeki katılaştırıcısı ile birlikte ticari olarak satılan silikon temelli bir polimerdir. PDMS 1:10 oranında katılaştırıcı ilave edilerek karıştırılmıştır ve silikon yonga plakası üzerinde bulunan SU-8'ten yapılmış erkek kanal geometrisi üzerine dökülmüştür. PDMS kanalın oluşturulması için hazırlanan SU-8 20 μm kalınlığındadır. SU-8 ticari olarak satılan bir negatif fotorezisttir ve fotolitografi yardımı ile karanlık maskeden kanal geometrisi silikon yonga plakasında oluşturulmuştur. PDMS kanal son işlem olarak akışkan girişi ve çıkışını sağlamak için mikro delgeç ile delinmiştir.

Oluşturulan elektrot ve PDMS kanalın birleştirilmesi için oksijen plazma altında yüzeyleri aktif hale getirilmiş ve sonrasında metil alkol ile kayganlaştırıcı tabaka oluşturularak mikroskop altında hizalanmıştır. Birleştirilen elektrot ve kanal vakum altına alınarak ısıtılmış ve alkol uzaklaştırılıp kuvvetli bir yapışma elde edilmiştir.

Bu işlemden sonra parçacıkların kanala yapışmasını engellemek için protein çözeltisi hazırlanmış ve bu çözelti kanal içerisinde bekletilmiştir. Sonrasında saf su ile kanaldan uzaklaştırılmıştır.

Yonga tabanlı sistemde akışkanın girişleri ve çıkışlarına ince borular takılmış ve bu borular mikro şırıngalara bağlanmıştır. Bu şırıngalarda mikro pompa olarak adlandırılan iticiler ile hareket ettirilerek kanalda akış sağlanmıştır. Elektrotlarda iki bileşenli iletken yapıştırıcı yardımıyla bakır kablolar ile sinyal jeneratörüne bağlanmıştır. Kanal tasarımında iki giriş ve iki çıkış mevcuttur ve bunların birine parçacık karışımı olan saf su, diğerine sadece saf su bağlanmıştır. Sonrasında floresan özelliği olan polistiren parçacıklar mikroskop altında asimetrik elektrik alandan geçirilerek incelenmiştir.

Deney simülasyonun yapıldığı voltaj ve akım değerlerinde yapılarak sonuçlar elde edilmiştir. Simülasyonun sonuçları deneylerin sonuçları ile örtüşmektedir ve bu simülasyonun doğruluğunu göstermektedir. Parçacıklardan 3.2 μm çapındaki kırmızı parçacıklar kanalın üst çıkışından, 9.8 μm çapındaki yeşil parçacıklar kanalın alt çıkışından çıkarak ayrıştırma sağlanmaktadır.

Comsol konferanslarında ve forumlarında kutupsal deviniminim 3 boyutlu olarak simüle edilmesi konusunda giderek artan bir çalışma yoğunluğu vardır ve bu çalışma örnek teşkil etmektedir.

Yapılan bu çalışma ile ayrıştırılması başarılan mikro parçacıklar gibi canlı hücrelerde ayrıştırılabilirler. Bu sistemler tasarlanırken Comsol ve Minitab gibi programlar kullanılarak tasarım zamanları düşürülebilir ve üretim öncesinde sistemler optimize edilebilirler. Ek olarak mevcut sistemler modellenerek farklı parçacıkların üzerindeki etkilerine bakılabilir veya oluşturulan geometrilerde iyileştirme çalışmaları yapılabilir.

TUBITAK tarafından 111M730 proje numarası ile desteklenen bu proje süresince ulusal ve uluslararası konferanslara özetler, makaleler yollanmış ve sunumlar yapılmıştır.

1. INTRODUCTION

1.1 Literature Review

LOC systems brings advantages, as they are cheap, needs very little analyze material, and has quick responses. These systems are focuses on diagnosis, treatment, drug delivery and environmental analyses. The market was valued at $2.6 billion in 2010 and is expected to reach $5.6 billion by 2015; growing at a Compound Annual Growth Rate (CAGR) of 16.7%. This growth is attributed to increasing applications specifically in cancer diagnostics and expression profiling, the boom in personalized medicine, and government funding (http://www.researchandmarkets.com/, 2011).

First scientist who had identified Dielectrophoresis (DEP) as dielectric particle movement under the non-uniform electric field was Herbert Pohl at 1950s. Pohl used the electrophoresis to discover the DEP, which was charged particle movement under electric field. In DEP particles does not have to be charged like in electrophoresis. Particles are interacted with the electric field in two ways: they travel to the high electric field region - positive dielectrophoresis (pDEP) or they pushed by the electric field to low electric field region - negative dielectrophoresis (nDEP). Electrical field frequency, particle and medium properties determines the particle response.

The progress in micro technology since last decades enabled microelectrodes with large electric field gradients and then with these gradients DEP forces applied on to the particles. There is no requirement for marking or modification in the particle, which directed scientists to use the DEP in cell manipulation. General approach on cells while the interested cell controlled by the pDEP the others suspended from the region of interest. In order to do this a continuous flow is required.

After 2000, the researches on DEP rapidly increased and tens of articles has been published on Lab-on-a-chip, Electrophoresis. Most of the articles has been published on United States of America and generally they are all multidisciplinary researches including physics, chemistry, biology, material sciences (http://www.scopus.com/, 2012). Carbon nanotubes (Arun, Salet, & Ionescu, 2011), nanoparticles (Lee et al., 2008), yeast cells (Cetin, Kang, Wu, & Li, 2009), polystyrene and micro particles

(Srivastava, Baylon-Cardiel, Lapizco-Encinas, & Minerick, 2011), blood cells (Kim & Yoo, 2009), cancer cells (Heller, Sullivan, & Krishnan, 2007), minerals (Du, Baune, Kück, & Thöming, 2008) are the generally investigated particles, cells.

1.1.1 DEP theory

The simplest theoretical model for DEP is that of a homogeneous spherical particle immersed in a dielectric medium. In a non-uniform electric field, the homogeneous spherical particle influences by a net dielectrophoretic force. The magnitude of this force depends on the polarizability of the particle with respect to medium as well as physical parameters and electrode setup. If a particle has polarizability higher than the medium, the DEP force will push the particle to regions of higher electric field see Figure 1.1 a) pDEP. If the medium has a higher polarizability than the particle, the particle will go to low field strength see Figure 1.1 b) nDEP.

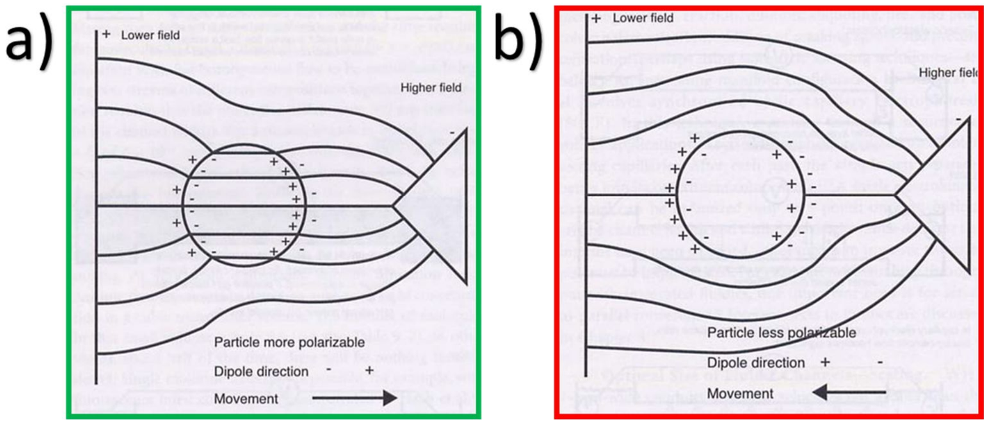

Figure 1.1 : Spherical particle under non-uniform electric field; a) pDEP, b) nDEP

In microscopic scale DEP force can be written as (Green, Ramos, & Morgan, 2002):

$$F_{DEP} = \mathrm{Re}[\rho(\omega)\nabla E] \quad \textbf{(1.1)}$$

In the equation E stands for the electric field, ω angular frequency (ω) corresponds to dipole momentum of the particle, which caused by the electric field and Re[…] corresponds to real part of the variables.

This equation becomes as below when its time average obtained:

$$\langle \mathrm{F}_{\mathrm{DEP}} \rangle = 2\pi a^3 \varepsilon_m \mathrm{Re}[k(\omega)]\nabla |E_{rms}|^2 \quad \textbf{(1.2)}$$

$\nabla|E_{rms}|^2$ gradient of electric field, k(ω) corresponds to Clausius-Mossotti (CM) factor which is stated as (Green et al., 2002),(Lungu, Neculae, Bunoiu, & Strambeanu, 2011), (Pethig, 2010),(Zhang, Khoshmanesh, Mitchell, & Kalantar-Zadeh, 2010):

$$k(\omega) = \frac{\tilde{\varepsilon}_p - \tilde{\varepsilon}_m}{\tilde{\varepsilon}_p + 2\tilde{\varepsilon}_m} \quad \textbf{(1.3)}$$

$\tilde{\varepsilon}_p$ and $\tilde{\varepsilon}_m$ are particle and medium dielectric constants. Dielectric constants obtained from the equation of: $\tilde{\varepsilon} = \varepsilon - j\sigma / \omega$ where $j = (-1)^{\frac{1}{2}}$. In this equation ε shows the dielectric permeability and σ shows the conductivity.

Clausius-Mossotti factor is the measure of the particle and medium relative permittivity. CM factor, depends on the applied electric field frequency, specifies the direction of dielectrophoretic force. According to equation (1.2) the dielectrical properties and diameter of the particle used for manipulating a particle.

DEP force decreases logarithmically from the surface of electrode and it reaches highest values at the edges of the electrodes. DEP force is proportional to square of the applied electrical potential. It also inversely proportional with the gap of the electrodes. If gap between electrodes divided by 10 then DEP for multiplied by 1000 (Green et al., 2002).

1.1.2 DEP devices

In general, DEP has application for numerous operations like separation, transportation, trapping, sorting and these operations enabled by the current photolithography techniques - microelectrode and microfluidic fabrication technologies. Separation by size, concentration, focusing, filtering, patterning also the other types of research areas in DEP.

Polystyrene particles, on the market and easy to obtain, are most preferred ones for development and design work. They are homogenous, sold with fluorescence properties with known diameters and electrical properties, and suitable for characterization of any DEP device.

In Figure 1.2 a simple design is captured with its electrical and fluidic connections where the purpose of the design was to focusing and trapping of 10 μm red fluorescent polystyrene spheres (Li et al., 2012) and in Figure 1.3 a design for sorting 10 and 5 μm polystyrene beads (Salomon, Leichlé, & Nicu, 2011).

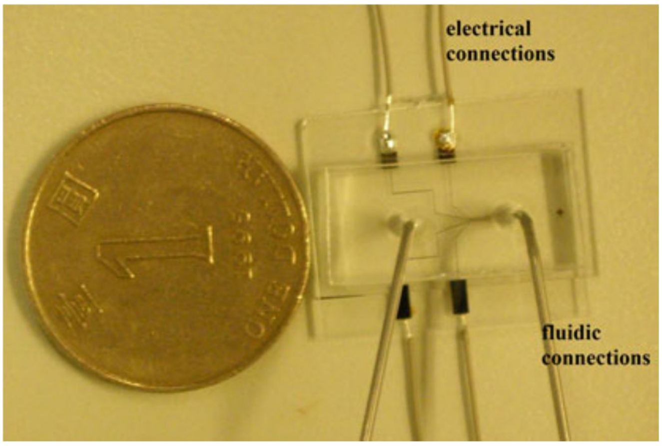

Figure 1.2 : Image of micro fabricated device (Li et al., 2012)

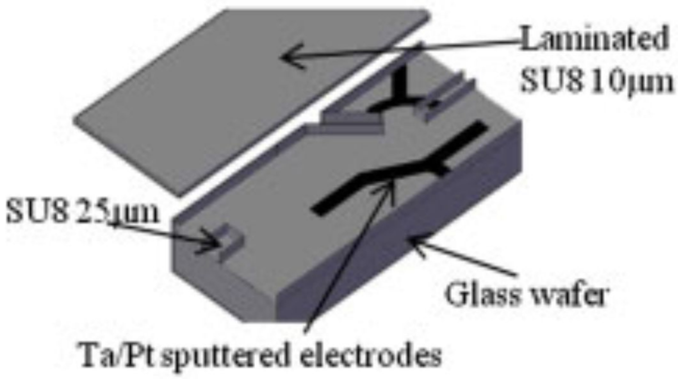

Figure 1.3 : 3D schematic of the device (Salomon et al., 2011)

As shown in the figures a general model for DEP devices consists of microfluidic channels and microelectrodes with their connections, which are generally, build on glass substrates. PDMS or SU8 materials has wide applications for micro channel fabrication and highly conductive metals like gold, titanium, platinum, aluminum, copper… electrodes mainly used for obtaining the required electric fields. Channel heights ranges from 10 μm to 200 μm, electrode thickness ranges differs from 10 nm to 1μm, sometimes for higher bonding to glass substrates 2 layers are used 1 layer which has better affinity with glass and 1 layer which has higher conductivity.

The literature reviews consist of many different electrode designs like parallel, castellated, oblique etc… Figure 1.4 shows the summary of electrode configurations which are built by the many researchers (Khoshmanesh, Nahavandi, Baratchi, Mitchell, & Kalantar-zadeh, 2011).

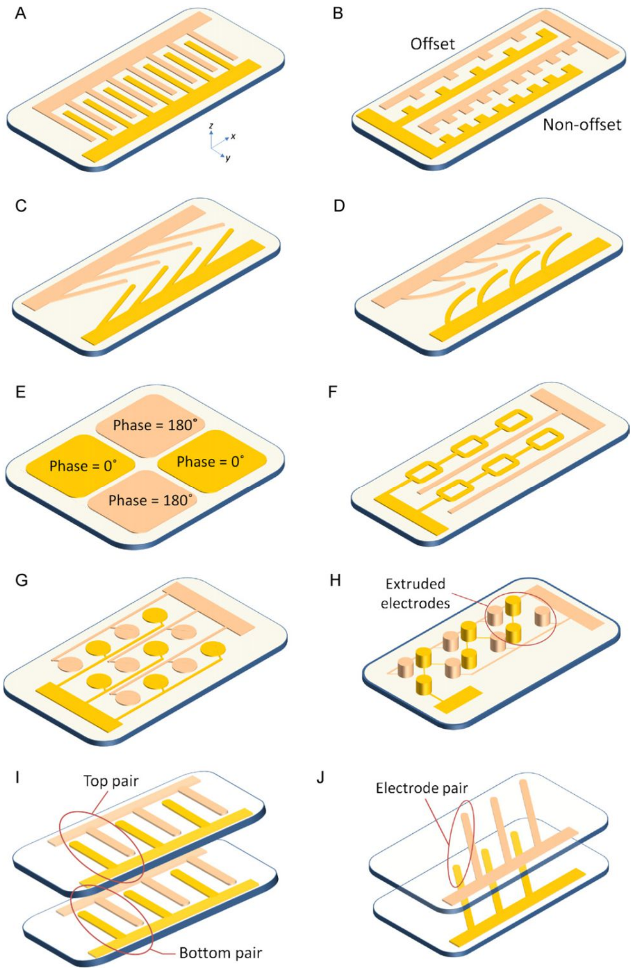

Figure 1.4 : Classification of DEP devices according to the configuration of microelectrodes: (A) parallel or interdigitated, (B) castellated, (C) oblique, (D) curved, (E) quadruple, (F) micro well, (G) matrix, (H) extruded, (I and J) top–bottom patterned (Khoshmanesh et al., 2011)

Dimensions of this electrode designs generally in the range of 10 μm to 100 μm electrode width and then a range of gap. Electrical potentials ranges from 1 V_{p-p} to 50 V_{p-p} and the frequency range is between 10 kHz to 10 MHz Polystyrene beads are generally suspended inside DI water(Khoshmanesh et al., 2011).

1.1.3 DEP device simulation theory

Microfluidic solutions for particle separation generally consist of design, fabrication and characterization steps and this leads to old style trial-error approach. Micro fabrication methods generally take several days to build a microfluidic device and may be another day to setup the experiment. Taking meaningful results almost took several weeks with the trial error approach. In order to improve designs and decrease the trial error time simulation of the systems becomes crucial.

Considering the DEP phenomenon electrical field, fluid flow, particle-tracing needs to be simulated, parameter optimization should be performed and design problems should be improved prior to fabrication and characterization of the DEP devices.

Comsol is a multyphysics program that can be simulate any kind of physical equation in any kind of geometry. 1, 2 and 3D simulations are possible with the lots of pre-installed modules. Comsol developers also researchers developed special module for microfluidics, which includes the Alternative Current (AC) / Direct Current (DC) , particle tracing, fluid flow in it.

Electrostatic in AC/DC can be a useful tool for simulating the electrodes and dielectrophoretic forces. Creeping flow in Microfluidics can simulate micro channels and drag forces. Particle tracing for fluid flow can simulate particle movement under the drag and dielectrophoretic forces and separation capability of a LOC device design. It can solve the static, time dependent, frequency dependent system.

1.1.3.1 Governing equations for DEP simulations

As previously stated DEP force is formulated as,

$$F_{DEP} = 2\pi r^3 \varepsilon_0 \varepsilon_m K \nabla |E|^2 \quad \textbf{(1.4)}$$

Where the electric field is the gradient of the voltage as in following formula,

$$E = -\nabla V \quad \textbf{(1.5)}$$

DEP force is directly changing with the gradient of the applied voltage. CM factor (K) that depends on the relative permittivity of the particle (ε_p) and medium (ε_m) with the formula of,

$$Re(f_{CM}) = Re[({\varepsilon_p}^* - {\varepsilon_m}^*)/({\varepsilon_p}^* + 2{\varepsilon_m}^*)] \quad \textbf{(1.6)}$$

Cube of the particle diameter is also changing the DEP force. In the continuous flow separation model the other force that influences the particle is drag force,

$$F_{drag} = \frac{1}{\tau_p} m_p (u - v) \quad \textbf{(1.7)}$$

The drag force changes with the mass of the particle (m_p), velocity response time (τ_p), particle velocity (v) and fluid velocity (u). In order to manipulate the particle DEP force should overcome the drag force.

1.1.3.2 Simulation steps in COMSOL

Many of the saleable software generally focuses on development of products but Comsol solves 3D multiphysics with finite element methods and the intention of the program is to help theoretical and experimental studies.

The simulation in Comsol starts with modelling of the physics, in DEP device simulation it starts with choosing the physical interactions like electrostatic, fluid flow, particle tracing. Then continuous with the creation of geometry and defining the materials and properties of the materials. Similar to all numerical solution methods boundary conditions, initial conditions assigned before the mesh creation for finite element methods. After that, solver configuration and solution requirements entered to the model like time and error range. Next step is to initiating the solver that creates the results and use the resulting data to create graphs for the reports.

1.1.4 Theory and application of the Statistical approach for Comsol model

Statistical software can be used to optimize the parameters of a system. Comsol also has optimization module in it but it is complicated and requires a high capacity computer. Instead of using the optimization module in Comsol, response surface design in Minitab statistical software can be used with the parameters of the model and a response from the Comsol with the given parameters can be entered in to the statistical analyze software to get a model and make optimization.

Response surface methods enables finding factor settings (operating conditions) that produce the "best" response, factor settings that satisfy operating or process specifications, identify new operating conditions that demonstrated improvement, model a relationship between the quantitative factors and the response (Montgomery, 2013).

In order to guess the response of the model with different parameters (factors) a linear function of the factors fitted with the results of the simulation model, the first-order model for the response surface design can be formulated as:

$Y = b_0 + b_1X_1 + b_2X_2 + ... + b_kX_k + e$

where Y = response, X = factors, b_k = regression coefficients, and e = error term with a normal distribution, mean of 0, and standard deviation of s. In here the coefficients for the parameters $b_{k,}$ are the estimates of the population regression coefficients, b_k. The estimated coefficients are used, along with the factors, to calculate the fitted value of the response. In matrix terms, the vector of coefficients in multiple regression is calculated by the formula:

$\mathbf{b} = (\mathbf{X'X})^{-1} (\mathbf{X'Y})$

In this formula X is the design matrix, including the constant and Y is the response vector.

For the creation of these formulas and the coeffients, Minitab generates a design matrix for each design. The first column is a column of one's for the constant term. This is followed by one column for each factor. If the model has squared terms, there is one column for each squared term. The column for a squared term is the product of the corresponding factor with itself. If the model has cross terms, then there is one column for each cross term. The column for a cross term is the product of the two different factor which are in interaction with each other. While creating the response surface design you can pick the interactions, you want to include in the design. If some squared or interaction terms removed due to data cannot support them, these will not be in the stored design matrix. The columns stored match the coefficients that are printed. Storing the design matrix used by Analyze Response Surface Design allows you to use other Minitab commands or you can change the order of the experiments and update the design matrix.

Furthermore, desirability for the response is calculate and an optimization interface generates the editable model and by using that optimizer, one can change the factors and generate the new responses.

Steps for response surface design:

- Create a response surface design by the previously determined parameters
- Name the factors and enter the parameters in to the model
- Make the required experiments and then enter your response on to the Minitab
- Use analyze response surface design to fit a model to the response data
- Then use response optimizer or use the created formula that belongs to the model to optimize the parameters or define new parameters for new requirements that gives the best response (Cornell, 1987).

2. DESIGN OF CONTINOUS FLOW DEP DEVICE

2.1 Device Design

In the early stages of research static simulations and designs has been done, interdigitated electrodes in a static chamber has been analyzed, and results are presented in another thesis. Because of that reason, static simulations and device designs will not be covered in this work. Chapter 1 summarized the theory behind the continuous flow particle manipulation and statistical approach to optimize parameters. Design work has been started with modelling in Comsol and systematically improvements applied to DEP based LOC device according the Comsol results. In all designs, material properties, and some of the parameters kept constant and some of them are considered as main variables and chosen for parameter optimization.
A new electrode design - angular interdigitated electrodes- modelled for the continuous polystyrene particle manipulation. The final design that is belongs to lithography process masks in order to fabrication the device shown in Figure 2.1, the colors indicate: Titanium Electrode, PDMS Micro channel, Glass Substrate (All dimensions are in microns).

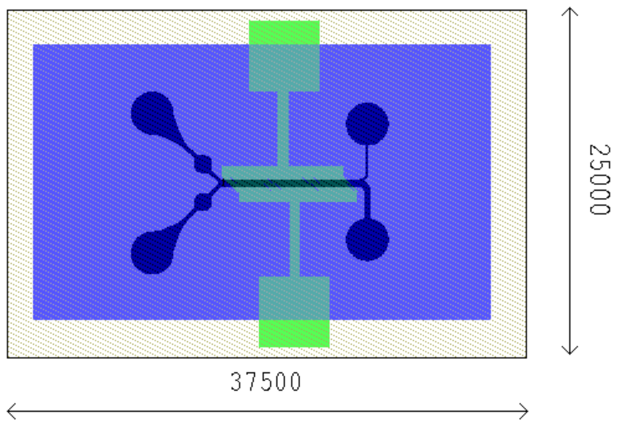

Figure 2.1 : DEP device LEDIT mask design

The design consist of 2 inlets, upper inlet for polystyrene particles and DI water mixture and lower inlet for additional feeding of DI-water to align both particles in the upper half of the channel see Figure 2.2.

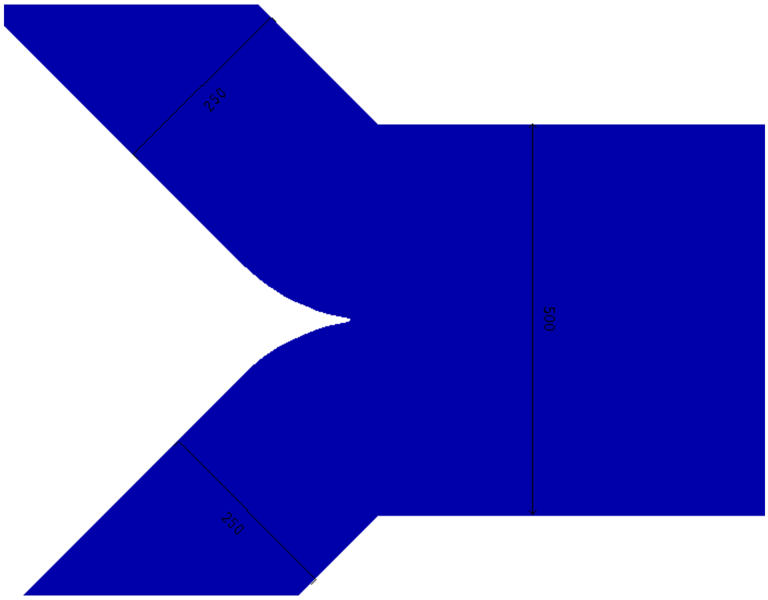

Figure 2.2 : Inlet details of DEP device (All dimensions are in microns)

2 outlets for different particles is shown in the Figure 2.3, upper inlet for the particles which are not affected by the DEP force and lower inlet for the particles manipulated by the DEP force.

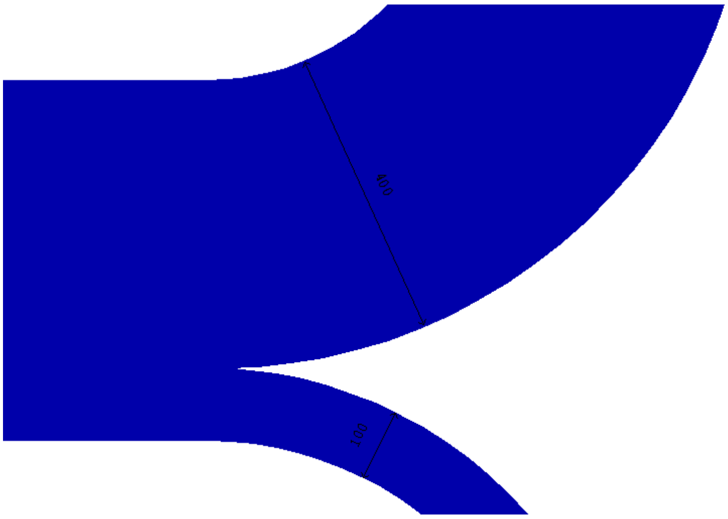

Figure 2.3 : Outlet details of DEP device (All dimensions are in microns)

Figure 2.4 shows the electrode configuration and dimensions of the electrodes the angles of the electrodes are 45 º and Figure 2.5, shows the electrodes when the voltage applied as positive to upper and negative to the lower electrodes.

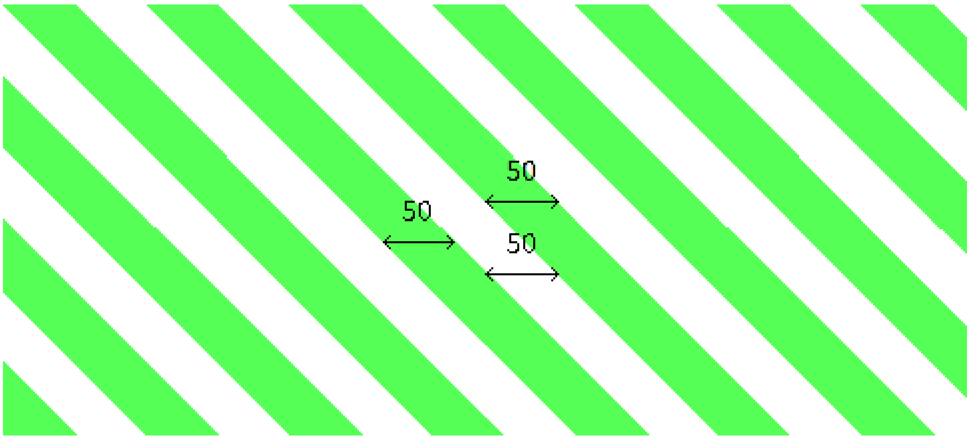

Figure 2.4 : Electrode details of DEP device (All dimensions are in microns)

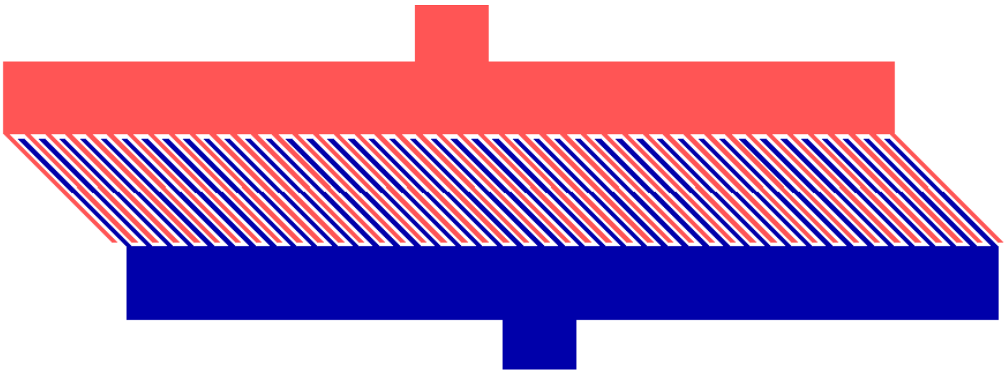

Figure 2.5 : Negative and Positive voltage in electrodes

Alignment of channel and the electrodes shown in the Figure 2.6 and channel positioned in the center of the electrode couples.

Figure 2.6 : Detail of electrode and channel alignment3D Model of The Device

2.2 3D model and Model theory

In order to demonstrate the design better a 3D CAD model designed and Figure 2.7 shows the 3D CAD model of the device. It includes the electrodes, microchannel, electrical connections, inlets and outlets of the channel.

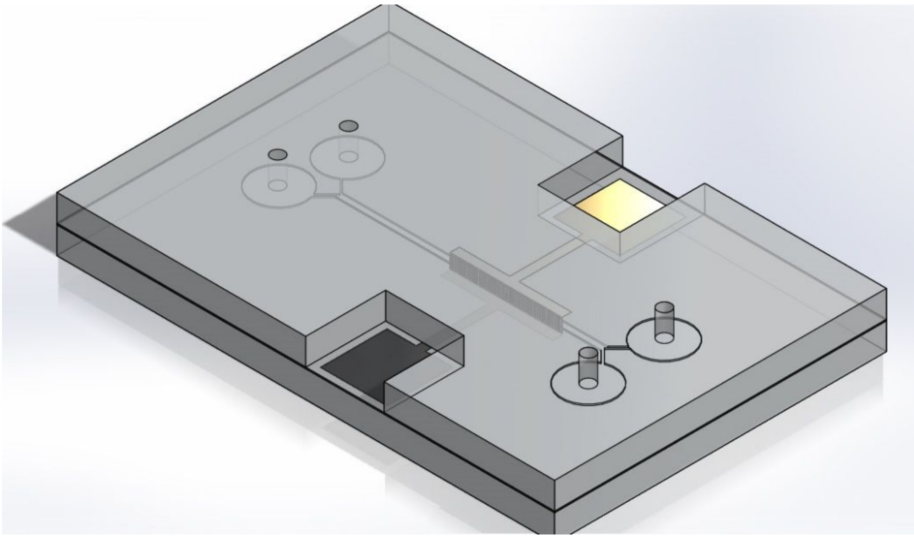

Figure 2.7 : 3D CAD model of the device

Figure 2.8 shows the representative side view of the device and demonstrates the configuration inside the channel. Flow, electrode couples, PDMS mold, and glass substrate configuration can be seen from the figure. Flow occurs at the top of the electrodes, which are loaded with electric potential, and PDMS guides the flow over the channel.

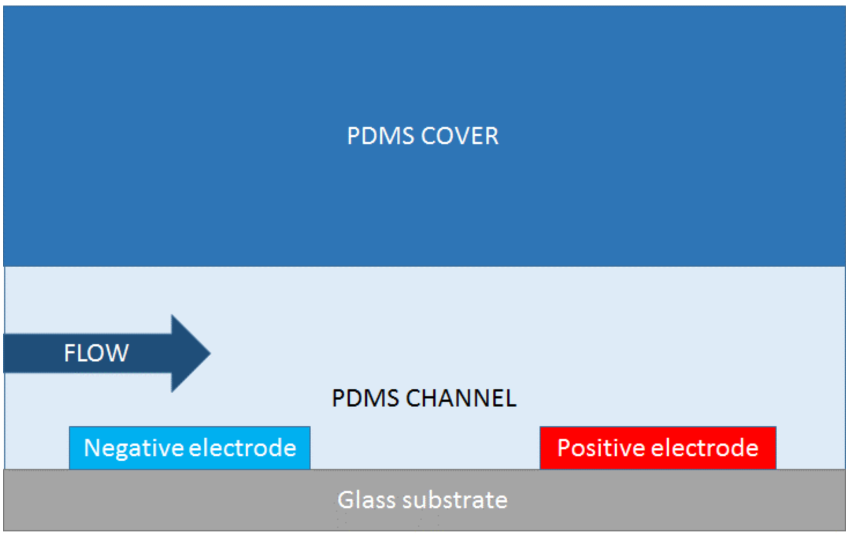

Figure 2.8 : Representative side view of the device

In order to understand the approach of the design, Figure 2.9 shows the representative top view of the channel and the acting forces according to the angular interdigitated electrode configuration.

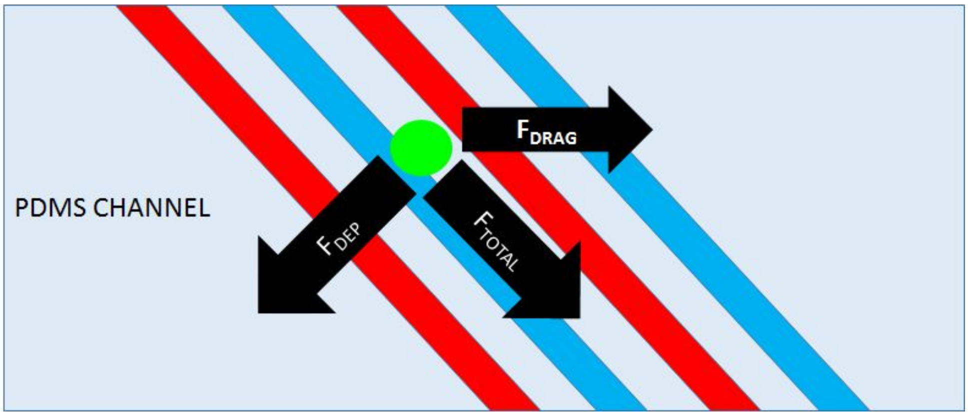

Figure 2.9 : Acting forces on particle

The forces in Figure 2.9 should be in balance in order to manipulate the particle in the direction of total force and this will enable the design to separate the particles from each other. Parameters like voltage, flow rate, channel height determines the manipulation amount of the particles. For separation purpose, one particle should be under the influence of DEP force and one should not be effected by DEP force. The particles are chosen as 3.2 μm (Red fluorescent) and 9.8 μm (Green fluorescent). They will be manipulated under a fluorescent capable microscope to observe particle movements.

3. COMSOL SIMULATION MODELS

In this section, simplified version of the described design for statistical analyzes will be introduced and then 1 to 1 model will be shown. The results will be shared in the 5th chapter.

3.1 Simplified Comsol model

Figure 3.1 shows the simulation model geometry in Comsol software. Two inlet and two outlet has been configured and angular electrodes modeled as a layer due to nanoscale thickness of the electrodes compared to micro channel.

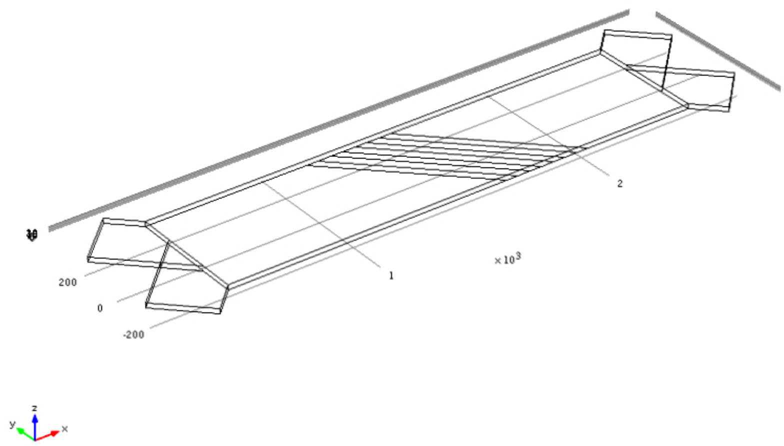

Figure 3.1 : Basic simulation model geometry

The width of the inlets and outlets are the half of the channel width that is 250 µm. Negative and positive electrode couples only modeled, first electrode and third electrode is under the positive potential load and second and forth is under the negative potential load.

Constant parameters in simplified model given in Table 3.1, which includes particle and medium properties and channel, dimensions.

Table 3.1 : Constant parameters in design

Constant parameters				
Channel length (µm)	**Electrode couple #**	**Electrode width (µm)**	**Relative Permittivity of DI water**	**Relative Permittivity of polystyrene particles**
2000	2	50	120	2.55
Channel width (µm)	**Density of water [kg/m^3]**	**Density of polystyrene particles [kg/m^3]**	**Electrode angle °**	**Height (µm)**
500	1000	1050	45	20

Solution of basic model with parameters in Table 3.2 will be covered in details at the 5th chapter and same simulations will be done for the other parameters in response surface design, which are shown in Table 3.5.

Table 3.2 : Simplified model simulation parameters

Flow rate (µl/min)	**Velocity (m/s)**	**Potential Vmax (V)**	**Particle diameter (µm)**
9	0.03	10	3.2
9	0.03	10	9.8

Electric field has been simulated in electrostatics module and Zero charge boundary condition assigned to the all surfaces except the electrode surfaces charge conservation for the model applied to the all model.

Laminar – incompressible flow has been chosen as a flow simulation model, except the inlet and outlets, slip boundary condition applied to the all surfaces.

For particle trajectories, particle tracing for fluid flow has been chosen as a model and bounce boundary condition applied to the walls except the inlets and outlets. Thirty particles released from the upper inlet, random initial position according to surface plane has been given and initial velocities collected from the flow model. Outlets has the freeze boundary condition to visualize the particles at the outlet.

The mesh for the model can be seen in Figure 3.2, which is a fine mesh, and Table 3.3 has the details of the mesh that consists of tetrahedral and triangular elements. Average element quality is higher than 0.1 which is an acceptable level (Ye & Daniels, 2011).

After completing creation of geometry, boundary condition assignment, parameter entrance and meshing, next step is to complete simulation.

Table 3.3 : Mesh properties

Property	Value
Minimum element quality	0.1831
Average element quality	0.7424
Tetrahedral elements	514841
Triangular elements	73146
Edge elements	2410
Vertex elements	52

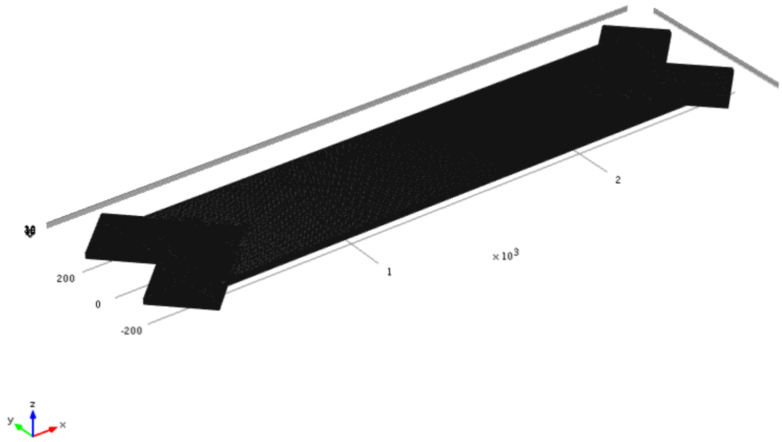

Figure 3.2 : Mesh of the geometry

Three studies have been used, first one is for electric field that performed with electrostatics, second one is laminar flow in order to obtain velocity field and the last one is particle tracing for fluid flow in order to obtain particle trajectories in the model.

3.2 Statistical Optimization of The Simplified Comsol Model

In order to make a statistical optimization with the simplified Comsol model, introduced simplified model used for all simulations at the parameters in Table 3.5. In order to create meaningfull results for creating responses, separation percentages has been calculated according to particle position changes by collecting average particle position changes in the first and last time step of solution in y direction. After that step, separation percentages used as responses of the simulation model and response surface analyze conducted with Minitab software. The results of the statistical optimization presented in the 5th chapter.

Table 3.4 : Response surface design parameters

Design \ Parameter	Flow rate (µl/min)	Potential Vmax (V)	Particle diameter (µm)
3 level 3 factorial design parameters for response surface design	0.6	1	3.2
	4.8	5.5	6.5
	9	10	9.8
RESPONSE SURFACE PARAMETERS & RUN ORDER 1 sided angular electrodes 45 ° 2IO Design	**Flow rate**	**Potential**	**Particle diameter**
	0.002	1	3.2
	0.03	1	3.2
	0.002	10	3.2
	0.03	10	3.2
	0.002	1	9.8
	0.03	1	9.8
	0.002	10	9.8
	0.03	10	9.8
	0.002	5.5	6.5
	0.03	5.5	6.5
	0.016	1	6.5
	0.016	10	6.5
	0.016	5.5	3.2
	0.016	5.5	9.8
	0.016	5.5	6.5
	0.016	5.5	6.5
	0.016	5.5	6.5
	0.016	5.5	6.5
	0.016	5.5	6.5
	0.016	5.5	6.5

3.3 Realistic Comsol Model

In this section, realistic version of the described design will be modeled with Comsol. Figure 3.3 shows the simulation model geometry in Comsol software. 2 inlet and 2 outlet has been configured and angular electrodes modeled as a layer due to nanoscale thickness of the electrodes compared to micro channel similar to simplified model. The width of the inlets are the half of the channel width that is 250 µm and they have fillets in the entrance. The outlets are asymmetric, the lower one is 150 µm, and upper one is 350 µm. Negative and positive electrode couples modeled as odds - negative and evens - positive.

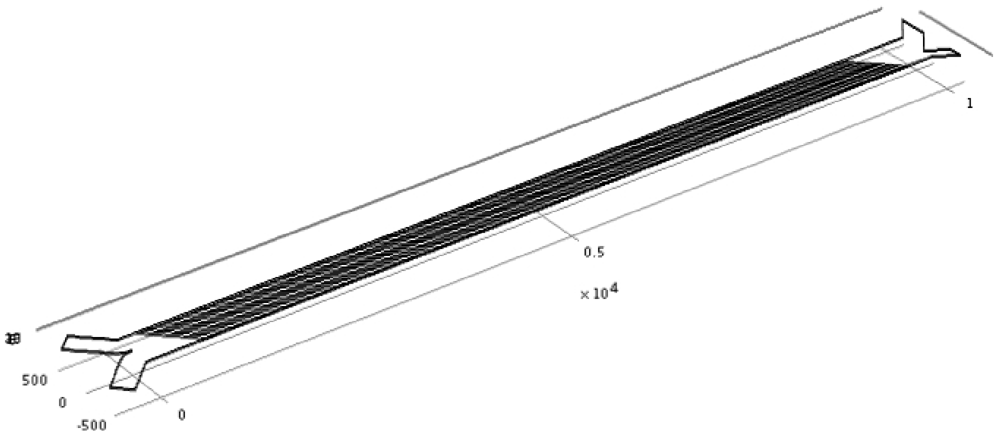

Figure 3.3 : Geometry of the realistic simulation model

Electrostatics, laminar – incompressible flow, particle tracing for fluid flow used with the same boundary conditions in simplified model simulation. The main difference is the geometry and all assumptions are replicated in that model too. Constant parameters in realistic model given in Table 3.5.

Table 3.5 : Constant parameters in realistic model

Constant parameters				
Channel length (µm)	**Electrode couple #**	**Electrode width (µm)**	**Relative Permittivity of DI water**	**Relative Permittivity of polystyrene particles**
10000	43	50	120	2.55
Channel width (µm)	**Density of water [kg/m^3]**	**Density of polystyrene particles [kg/m^3]**	**Electrode angle (°)**	**Height (µm)**
500	1000	1050	45	12.5

Solution of realistic model with parameters in Table 3.6 will be covered in 5th chapter and will be the experimental study inputs as well.

Supply of the DI water will be done with a syringe pump in the experimental setup, which is working with the flow rate, and the simulation model works with the inflow velocity and because of that reason a conversion is needed and it is demonstrated in Table 3.6 (Flowrate x Area = Velocity). The values on that table will be the inflow velocity in simulation and in experimentation; they will be used as flowrate.

Table 3.6 : Realistic model simulation parameters

Height (µm)	Voltage (V)	Width (µm)	Flowrate -Q (µl/min)	Flowrate-Q (µm³ / min)	Area - A (µm²)	Velocity (µm/min), V=Q/A	Velocity (m/sec)
12.5	1	250	10	10000000000	3125	6400000.00	0.11
12.5	1	250	20	20000000000	3125	12800000.00	0.21
12.5	5	250	10	10000000000	3125	6400000.00	0.11
12.5	5	250	20	20000000000	3125	12800000.00	0.21
12.5	10	250	10	10000000000	3125	6400000.00	0.11
12.5	10	250	20	20000000000	3125	12800000.00	0.21

The mesh for the model can be seen in Figure 3.4, which is a normal mesh, and Table 3.8 has the details of the mesh that consists of tetrahedral and triangular elements. Realistic model solved similarly, geometry creation, boundary condition assignment, parameter entrance and meshing followed by solvers of three studies as electrostatic, laminar – incompressible flow and particle tracing for fluid flow.

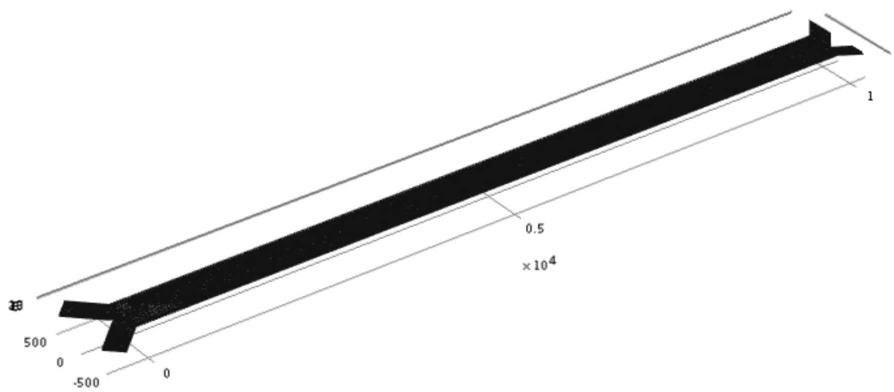

Figure 3.4 : Mesh of the geometry

Table 3.7 : Mesh properties of Realistic model

Property	Value
Minimum element quality	0.18563
Average element quality	0.652
Tetrahedral elements	37647
Triangular elements	26304
Edge elements	4915
Vertex elements	376

4. DEVICE FABRICATION AND EXPERIMENTAL SETUP

Fabrication of the design performed with photolithography techniques. LOC device consist of glass substrate, titanium electrodes, PDMS micro channels, electrical and fluidic connections. In photolithography, required patterns for microelectrodes, transferred to the glass substrate with using masks and patterns for PDMS micro channels obtained via micro replication, which obtained by using masks and silicone -wafers in order to obtain male profile for the channel groove.

Photoresist, which is a photosensitive chemical material, is spin coated on to the glass or silicon wafer and then with the application of UV light, permanent patterns obtained. There are mainly two types of photoresists exist (See Figure 4.1), positive and negative, mask designs are adjusted according to either one of them. After photo activation, substrates are agitated under the developer of the photoresist and final pattern obtained.

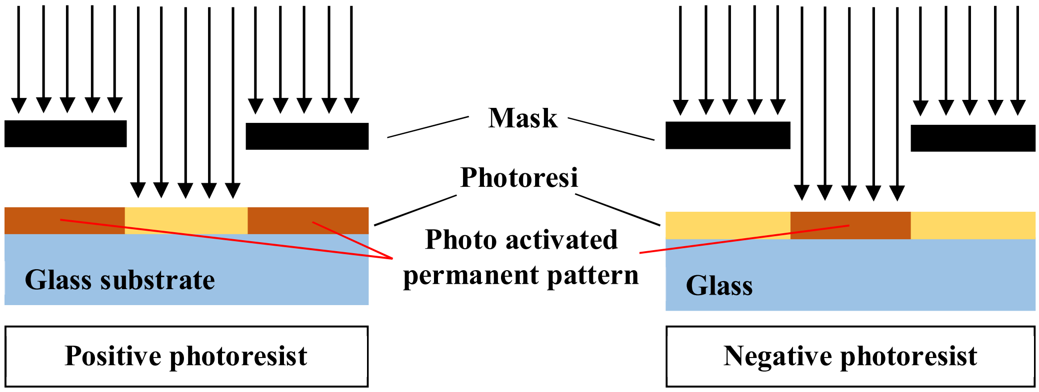

Figure 4.1 : Positive and Negative photoresist

Physical Vapor Deposition – PVD used for evaporating a target material and then coating it on the substrate. In order to reduce the contamination this process performed at high vacuum medium. PVD method precision in coating ranges from angstrom level to nano level. The explained fabrication methods used for the fabrication of the previously introduced device design.

4.1 Electrode Fabrication

In order to obtain the pattern of the electrodes, glass substrate cleaned with 1 molar KOH solution under the sonicator for 10 minutes and then washed with acetone before the photoresist coating process. Positive - AZ 1505 photoresist (AZ Electronic Materials) has been spin coated (Laurel WS-400E9) on glass substrate which thickness adjusted to 400nm by the spin coating parameters and photoresist specification sheet. Photolithography process performed with OAI Model 200 Mask Aligner under MID UV (260nm-325nm) light.

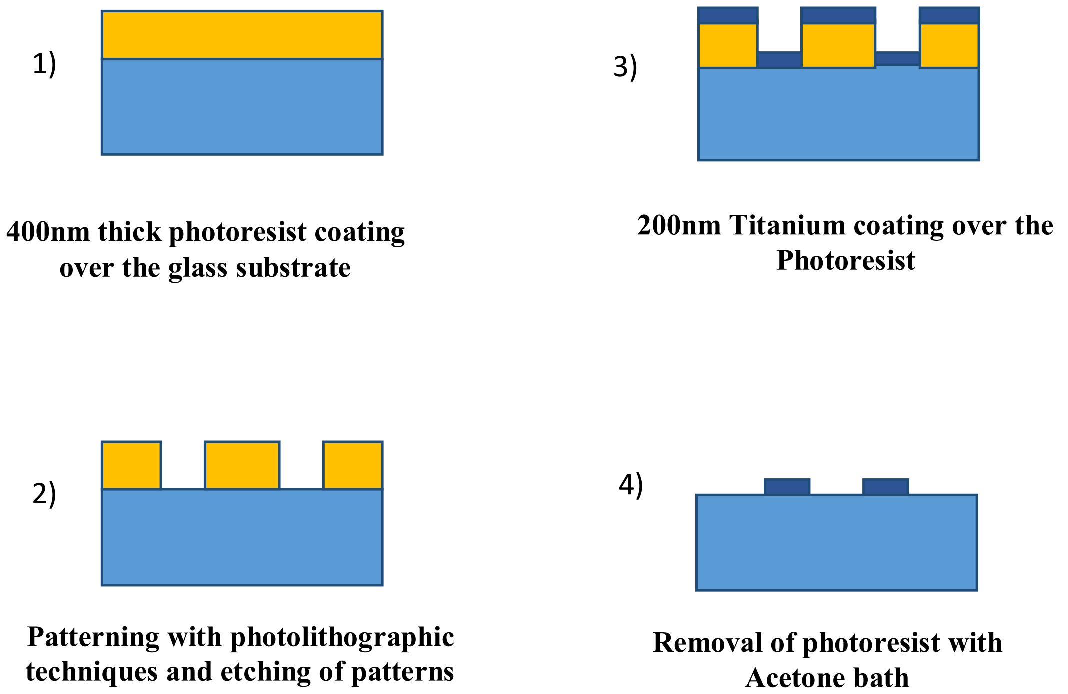

Figure 4.2 : Electrode fabrication process steps

Multi-PVD (Öncel İleri Malzeme Teknolojileri) with electron beam (E-beam) used to evaporate the Titanium target and coat it over the glass substrate that patterned with photolithography techniques. With this method 200 nm thick titanium coated over the photoresist coated glass substrates and then photoresist removed with acetone bath and the final electrode pattern obtained over the glass substrate. Steps schematically explained in Figure 4.2 and obtained final electrode shown in Figure 4.3.

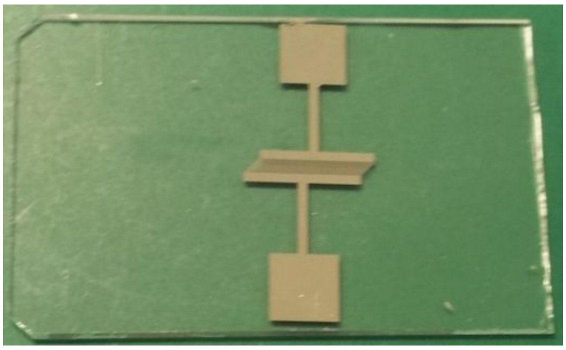

Figure 4.3 : Fabricated electrode sample

4.2 Micro Channel Fabrication

Similar to electrode fabrication, photolithography techniques used to obtain the male pattern of the micro channel groove. SU-8 Negative photoresist coated over a silicon wafer and then the channel pattern transferred from a dark field mask and inactive SU-8 removal performed and the mold for micro replication obtained (see Figure 4.4).

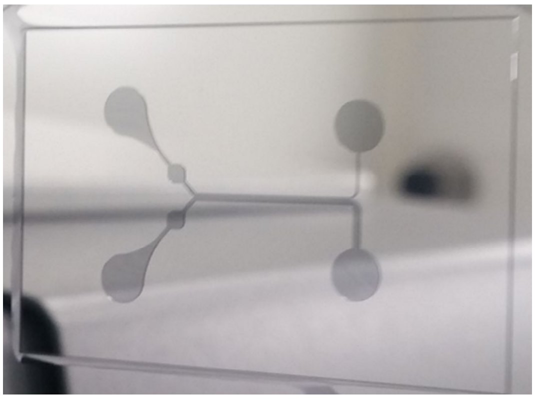

Figure 4.4 : SU-8 mold for micro channel

After that, PDMS is casted over that SU-8 mold and then left for solidification. Finally, the PDMS layer removed from the SU-8 mold and micro channel pattern obtained. SU-8 mold height measured as 12.5 μm with the AXIO CSM 700 confocal microscope. Before assembly, drilling performed with Harris Unicore 0.75mm punch for the fluidic connections (See Figure 4.5).

4.3 Assembly

PDMS micro channel and electrodes over the glass has been assembled using oxygen plasma process. The bonding surfaces taken under the oxygen plasma with Harrick Plasma cleaner and then, they aligned under the microscope with application of methanol for easy aligning. After that, the assembly placed under the vacuum for removal of the methanol under the 50°C for 15 min in the oven. Then bi component conductive epoxy (Circuit works) used to bond the electrical wires to the electrical connections of the electrodes. Figure 4.5 shows the LOC device, which is ready for the experimentation.

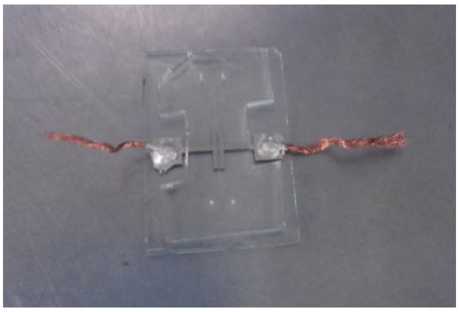

Figure 4.5 : Assembled device

4.4 Experimental Setup

Fabricated LOC devices connected to "81150A Pulse Function Arbitrary Noise Generator, Agilent Technologies, (ABD)" with the electrical connection cables. AC applied to the electrode couples (voltage x sin (wt) and voltage x sin (wt+ π)) at 2 MHz frequency. Particle mixture and DI water applied with "Harvard Pump 11 Plus Dual Syringe" pumps. Syringe pump flow rate entered according to the needle inner diameters (Hamilton Microliter Syringes) and fluidic connections completed with ELVEFLOW microfluidic kit. The elements of the experimental setup consist of Pulse generator, pumps, OLIMPOS BX41M fluorescence capable microscope and LOC device, which can be seen from the Figure 4.6.

Figure 4.6 : Experimental setup

Fluidic and electrical connection details can be seen on Figure 4.7. System is fixed to the microscope with tapes in order to prevent movement during analyzes.

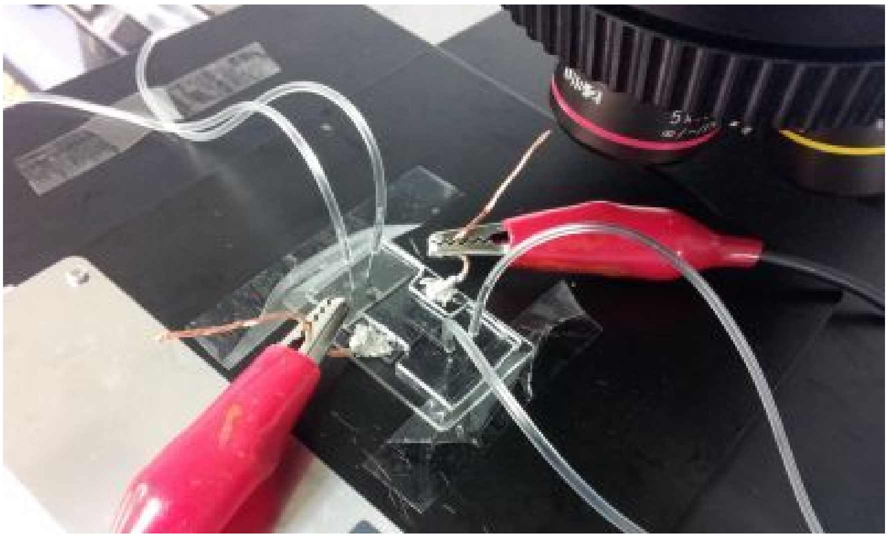

Figure 4.7 : Details of the connections

Table of the microscope can be adjusted in x, y and z-axis. Experiments performed under the 5-x magnification in order to see channel width. Focus adjusted with the knops in order to see polystyrene fluorescent micro particles. Polystyrene fluorescent micro particles, d=3.2 μm and d=9.8 μm, are added to DI water and the overall conductivity of the suspension was measured as 2.5x10-4 S/m with "HC 3010 Conductivity Meter, Trans Instruments (Singapore)".

4.5 Inhibiting fouling in microchannel

Early experiments showed non-specific adsorption of polystyrene microparticles, the problem reduced the visualization, and florescent microscope images directly affected from the stucked particles. Then the microchannel surface needed a surfactant and Bovine serum albumin (BSA) with Phosphate buffered saline (PBS) is used as for inhibiting the fouling of polystyrene microparticles (Arun et al., 2011; Nam, Kim, Park, & Park, 2013).

In order to obtain 1000 mL PBS, 10 g NaCl, 0.25g KCl, 0.9525g Na2HPO4, 0.09625g KH2PO4 weighted and added to the 100 ml distillated water. The concentrated solution agitated 1 hour to dissolve the salts in the distillated water. Then concentrated solution diluted with 900 ml DI water and agitated for 10 to 15 minutes and homogeneous solution obtained.

60mg BSA (Sigma-Aldrich) added to 30 ml PBS and then 30ml PBS added and 1mg BSA/1ml PBS solution obtained. The solution pumped in to the microchannel and washed with DI water after 24 hours in order to inhibit the fouling of the microparticles in the microchannel.

5. RESULTS AND DISCUSSION

In this chapter, simplified Comsol simulation model results, statistical optimization results, realistic Comsol model simulation results, experimental study results will be demonstrated and comparison of the realistic Comsol model results with experimental results will be covered. Finally, discussion of the results will be made.

5.1 Simplified Comsol Model Results

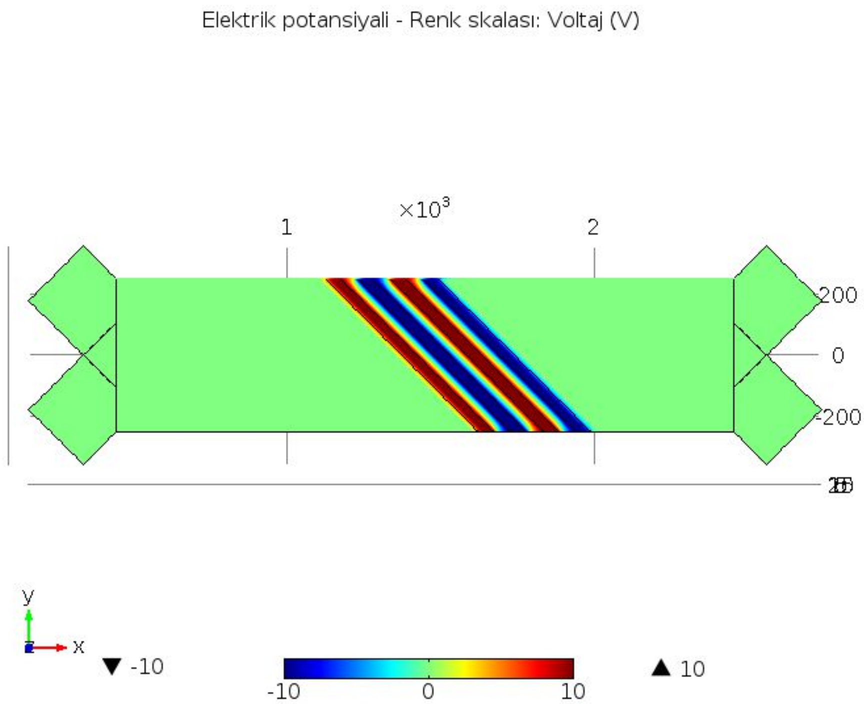

Figure 5.1 : Electric potential of the model

Electric potentials in the model shown in the Figure 5.1 that are coming from -10 and +10 volt load applied to electrode couples also shown in Figure 5.2. Only four electrode has been modeled which is only for demonstrating Comsol result and showing a statistical analyze model. Simulation of a complete model takes couple of hours and 20 simulations needs to be done for response surface design, which took too much time. With this simplified model, all simulations took couple of hours with a standard quad core computer. For similar analyzes in complete model a supercomputer is needed.

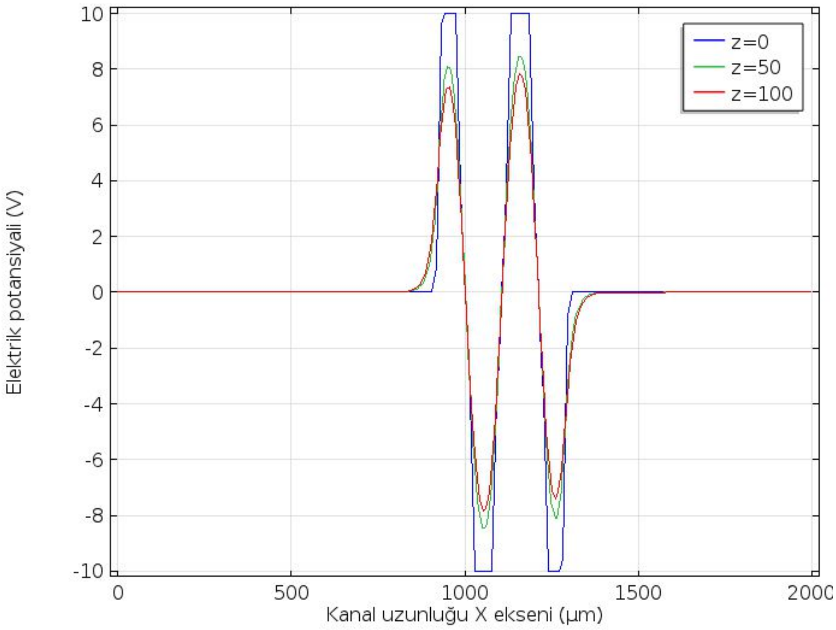

Figure 5.2 : 1D Electrical potential versus the channel length

The resulting electric field of electrical potential shown in Figure 5.3 and distribution along the electrodes has been given in Figure 5.4. Maximum electric field gradient is around 1.2x10^6 V m^{-1} and it occurs at the edges of electrode surface and reduces to 0.3x10^6 V m^{-1} at the top of the channel (Figure 5.4 shows the peaks). That gradient will be contributed to the DEP force as stated in design chapter and push the particles downwards as shown in the Figure 2.9.

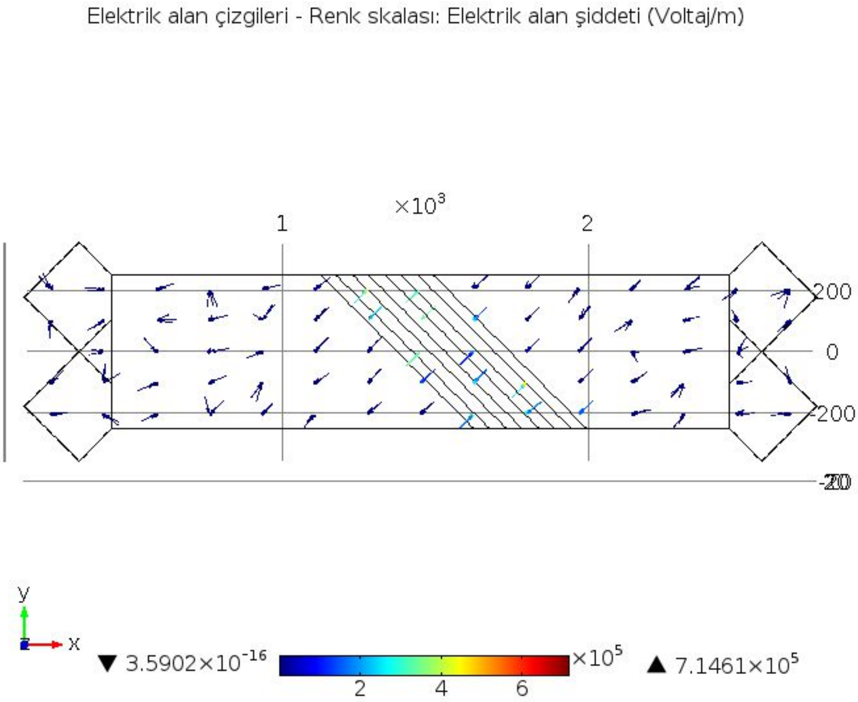

Figure 5.3 : Electrical field of the model

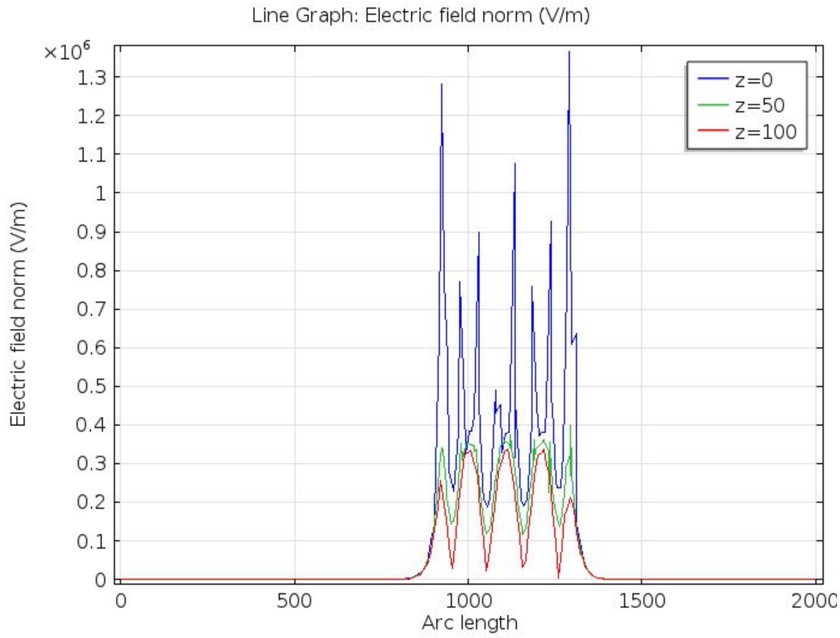

Figure 5.4 : Electrical field distribution along the channel length

Velocity field is shown in Figure 5.5 0.03 m/s is applied from the 2 inlets in the left side which are increasing the velocity in the mixing at the joint of 2 channels and reaching to 0.04m/s. The friction in micro channels neglected and slip boundary condition applied because of that the velocity is very similar near the channel walls Figure 5.6 shows the velocity profiles at different locations in the channel center).

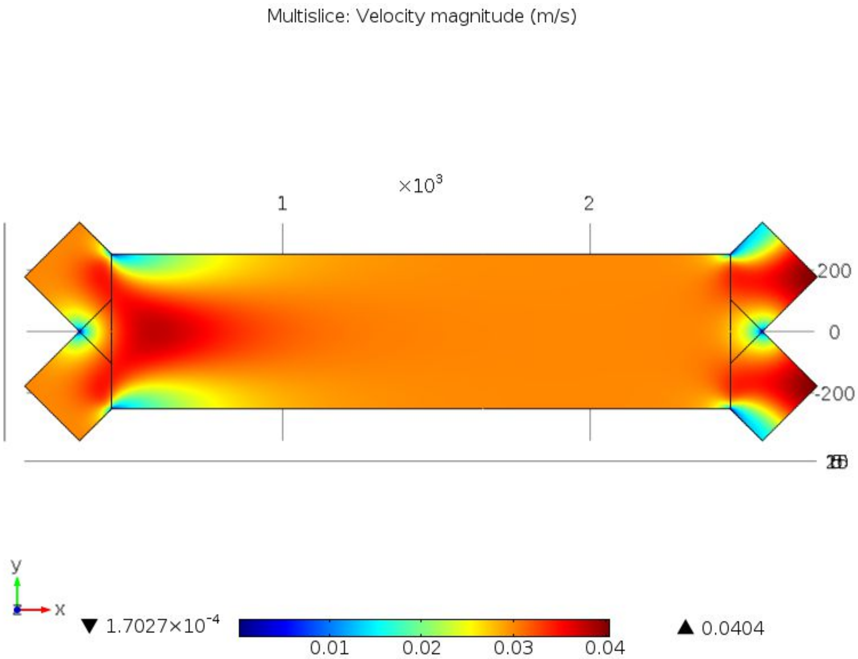

Figure 5.5 : Velocity field of the model

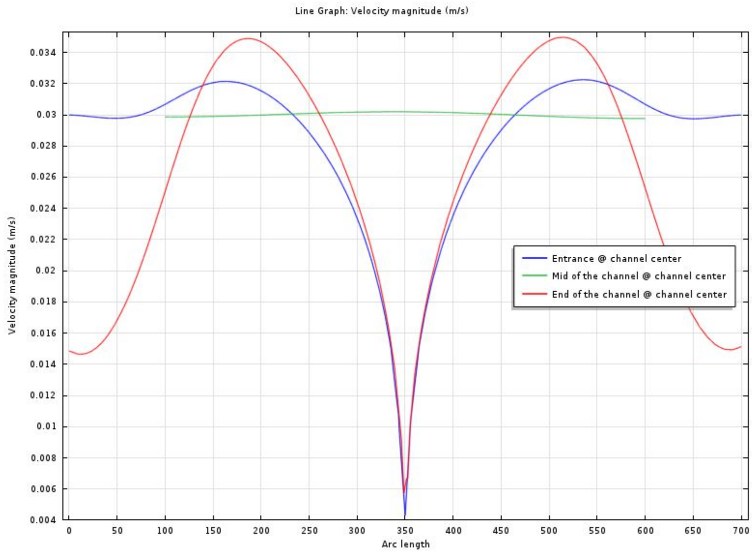

Figure 5.6 : 1D Velocity profile of the channel along the channel width

The generated electric field and velocity field coupled in to the particles and particle flow for fluid flow study performed with time dependently and particle trajectories obtained. In addition, parametric sweep for 3.2 µm: red fluorescent and 9.8 µm: green fluorescent implemented in to the study to solve both in one model and it will enable to obtain single image of both particles' trajectories. Figure 5.7 shows the particle trajectories at the end of the simulation. Applied parameters resulted in separation red particles leaves from the upper end of the channel and green ones leaves from the lower end of the channel. In order to create a meaningful result separation parameter is calculated by using the point average values of all particles.

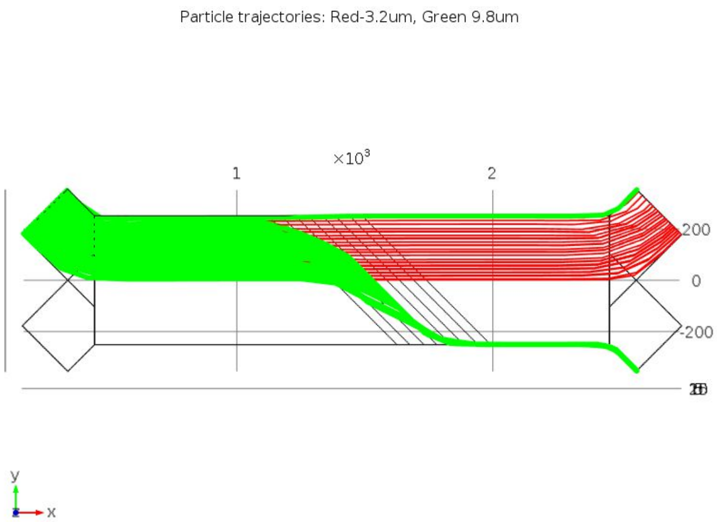

Figure 5.7 : Particle trajectories in model

Average of initial position has been subtracted from the final positions and divided by maximum of this position change (see Table 5.1). Figure 5.8 shows the particle position average in y direction along the channel and it shows that particles are separated and following different paths. Table 5.1 shows the separation percentages of the model according to the particle diameters and average of particle position in initial and final positions.

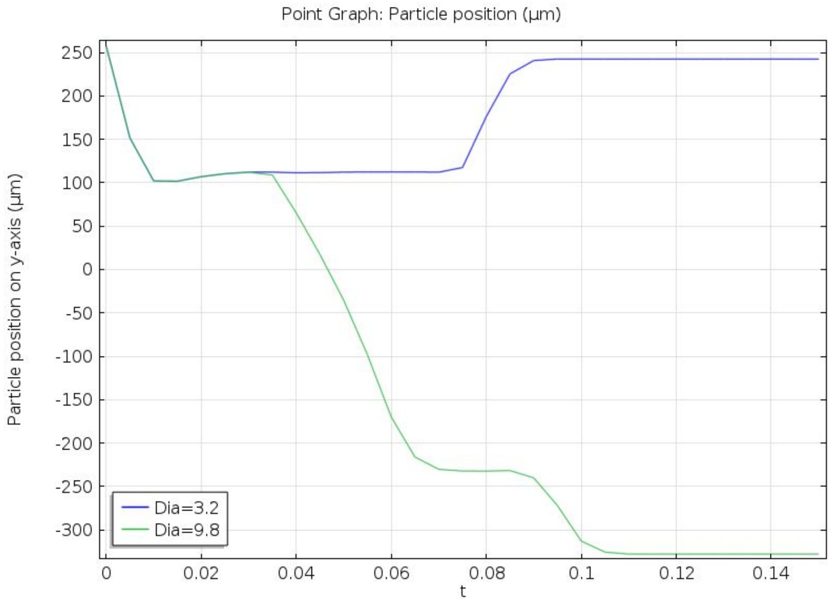

Figure 5.8 : Particle position change for the solution time in Y axis

Table 5.1 : Solution of demonstrated parameters

Flow rate (µl/min)	Velocity (m/s)	Potential Vmax (V)	Particle diameter (µm)	Separation percentage	Start position average (µm)	Final position average (µm)	Change in Point average of particle position in Y axis (µm)
9	0.03	10	3.2	0.024	259	246	13
9	0.03	10	9.8	1.000	259	-300	559

In order to understand this separation Figure 5.9 should be investigated, the dotted lines shows the X axis component of the drag force and straight lines shows the Y axis component of the DEP force which overcomes the drag forces x component and pushes the particles down in Y axis. The effect in 9.8 um particles are much higher and this is enabling the separation of the larger sized particle.

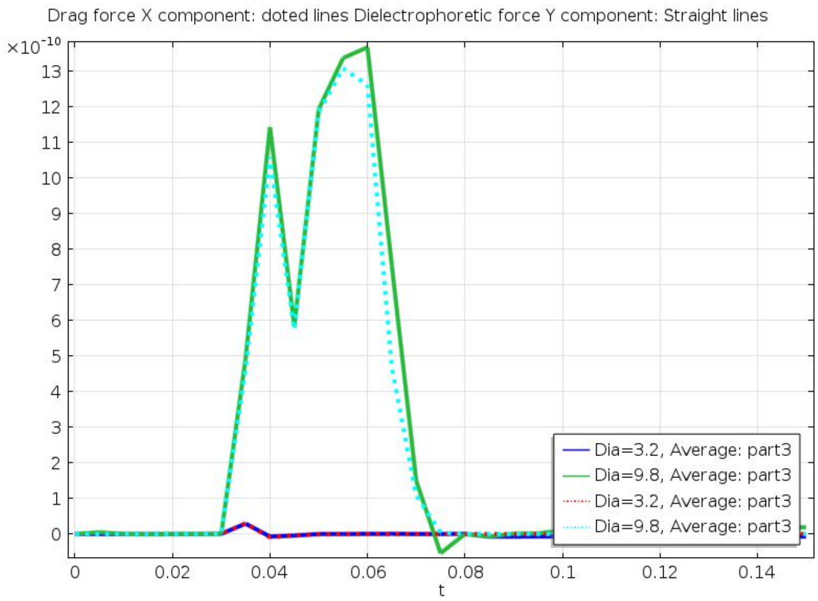

Figure 5.9 : Average DEP force acting on particles at Y-axis versus average negative of the drag force acting on particle at X-axis

The DEP force visualized in Figure 5.10 and 5.11 for green and red particles along the channel with the trajectories. Figures also demonstrates where the particles effected by the force most, electrode edges.

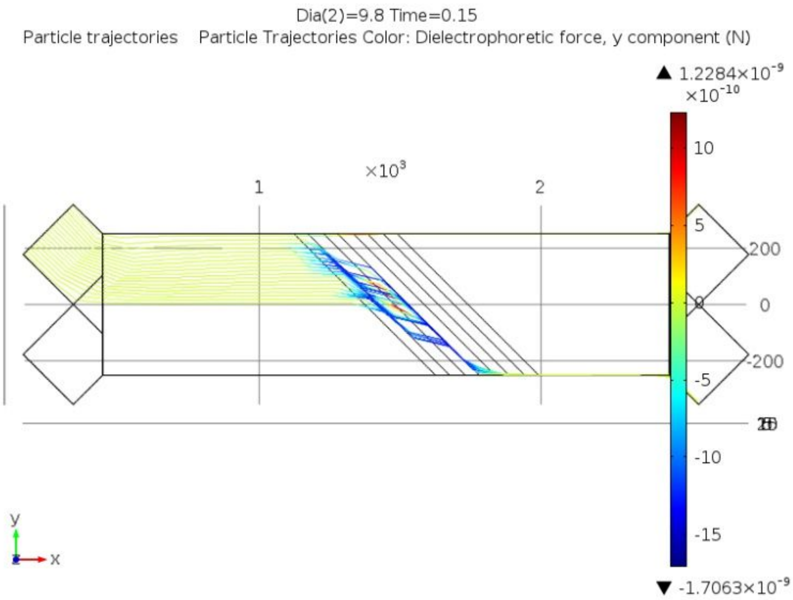

Figure 5.10 : Particle trajectories of 9.8 um particles with DEP force color scale

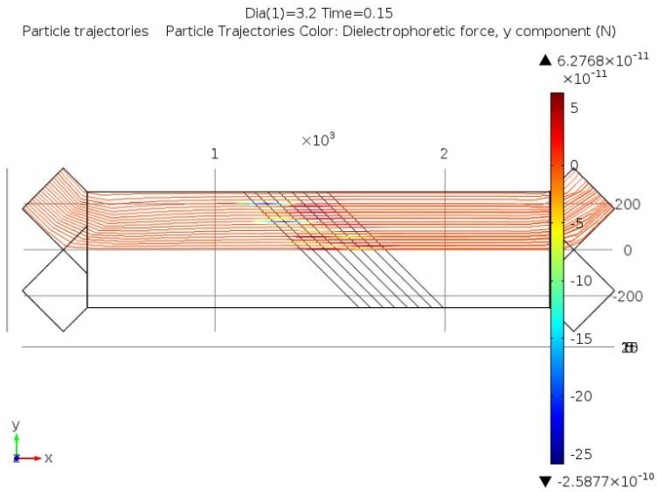

Figure 5.11 : Particle trajectories of 3.2 um particles with DEP force color scale

Another observation is particles are moving upwards in the channel height when they attracted by the electrode surfaces. Z component of DEP force causes this movement and it can be seen from the Figure 5.12, the time that the particles moves forward is directly matching the DEP force Z component magnitude shown in Figure 5.13.

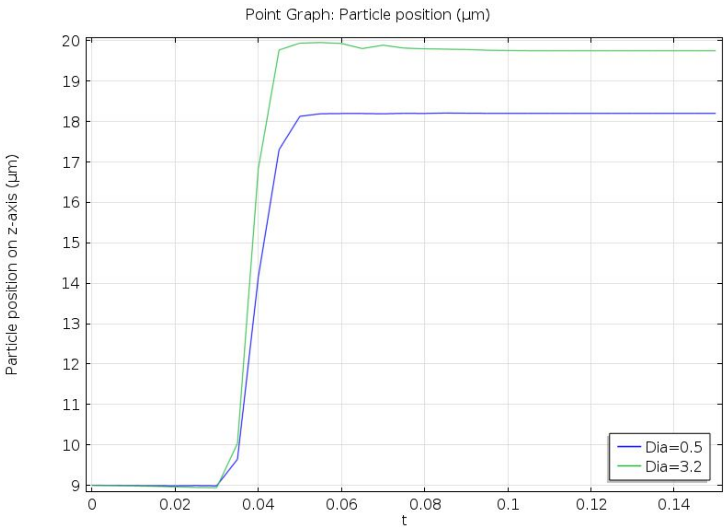

Figure 5.12 : Particle position change for the solution time in Z-axis

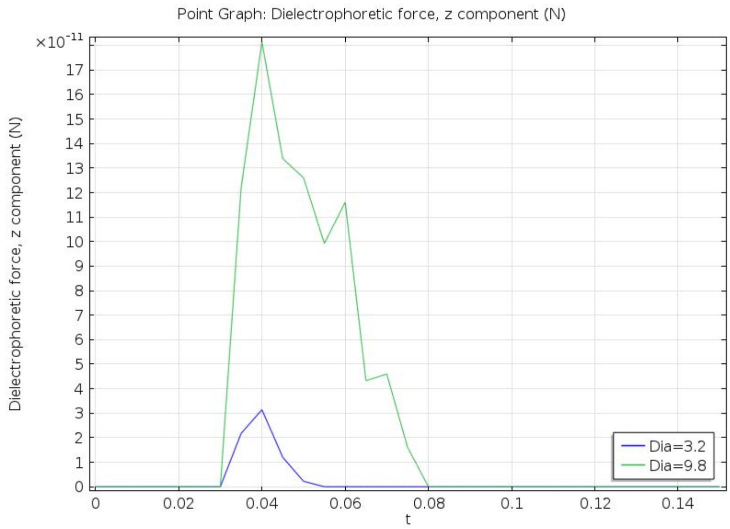

Figure 5.13 : Average DEP force acting on particles in Z-axis

5.2 Response Surface Design Optimization Results

The demonstrated parameters in 3rd chapter for response surface optimization in Minitab has been solved and results can be seen on Table 5.2. All the results are added to the Minitab and response surface model solver created an optimization model and equation which includes coefficients for the parameters and using the excel file, optimization equation is obtained. The equation can be used for different input parameters and separation percentage can be estimated (Model coefficients are shown in Table 5.3). Response optimizer tool in Minitab also used to shows the response optimizer results for the 3.2 and 9.8 µm particles. Left side of the Figure 5.14 shows the best separation percentage of 3.2 µm particles and right side shows the 9.8 µm particles.

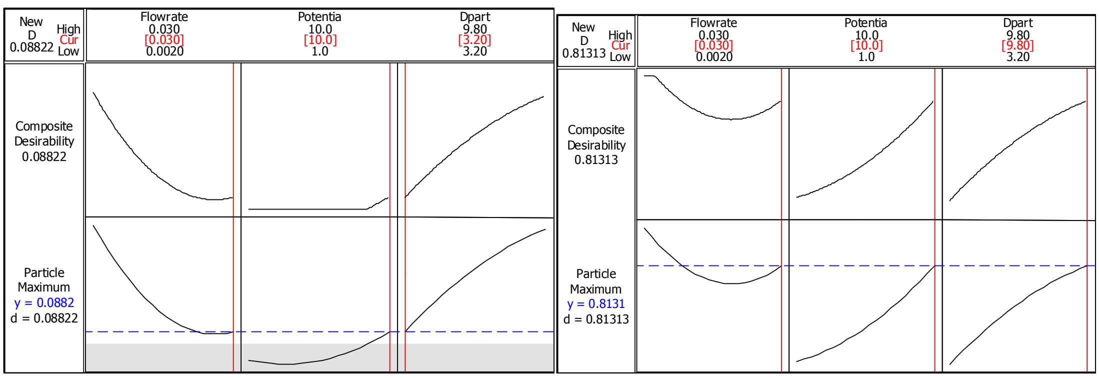

Figure 5.14 : Response surface optimizer results for 9.8 µm and 3.2 µm particles

Table 5.2 : Response surface design for particle separation optimization

Design \ Parameter	Flow rate (µl/min)	Potential Vmax (V)	Particle diameter (µm)	SOLUTION DETAILS				
3 level 3 factorial design parameters for response surface design	0.6	1	3.2	(Start-Final position)/(Max(Start-Final position)			(Start-Final position)	
	4.8	5.5	6.5					
	9	10	9.8					
RESPONSE SURFACE PARAMETERS & RUN ORDER 1 sided angular electrodes 45 ° 2IO Design	Flow rate	Potential	Particle diameter	Separation percentage	Start position average	Final position average	Point average of particle position in Y axis	Solution time
	0.002	1	3.2	0.016	258.96235	249.85023	9	0.1
	0.03	1	3.2	0.029	258.96235	242.99438	16	0.5
	0.002	10	3.2	0.881	258.96235	-233.17835	492	0.1
	0.03	10	3.2	0.024	258.96235	245.65807	13	0.5
	0.002	1	9.8	0.019	258.96235	248.5412	10	0.1
	0.03	1	9.8	0.026	258.96235	244.26863	15	0.5
	0.002	10	9.8	0.909	258.96235	-248.78751	508	0.1
	0.03	10	9.8	1.000	258.96235	-299.87346	559	0.5
	0.002	5.5	6.5	0.880	258.96235	-232.68176	492	0.1
	0.03	5.5	6.5	0.027	258.96235	243.95198	15	0.5
	0.016	1	6.5	0.050	258.96235	231.05321	28	1
	0.016	10	6.5	0.561	258.96235	-54.455	313	1
	0.016	5.5	3.2	0.024	258.96235	245.82153	13	1
	0.016	5.5	9.8	0.209	258.96235	142.02773	117	1
	0.016	5.5	6.5	0.051	258.96235	230.58584	28	1
	0.016	5.5	6.5	0.050	258.96235	230.95876	28	1
	0.016	5.5	6.5	0.052	258.96235	230.1583	29	1
	0.016	5.5	6.5	0.050	258.96235	230.94176	28	1
	0.016	5.5	6.5	0.051	258.96235	230.66608	28	1
	0.016	5.5	6.5	0.051	258.96235	230.56242	28	1

Table 5.3 : Surface response model for the separation percentage (Equation of the design)

Separation percentage (Summation of Coefficient*Contribution)			1.000
Term	Coefficient	Contribution	Coefficient *Contribution
Constant	0.25732	1	0.257
Flow rate	-60.786	0.002	-0.122
Potential	-0.0153	10	-0.153
Dpart	0.04864	9.8	0.477
Flow rate*Flow rate	1291.99	0.000004	0.005
Potential*Potential	0.0052	100	0.520
Dpart*Dpart	-0.0077	96.04	-0.738
Flow rate*Potential	-1.5582	0.02	-0.031
Flow rate*Dpart	2.55313	0.0196	0.050
Potential*Dpart	0.00845	98	0.828

Statistical approach can be used for different designs and Comsol results can be converted to responses with this approach and a simple excel can solve the resulting equation. Statistical approach only demonstrated as a novel approach it will not going to be replicated in the realistic Comsol model because of the limited hardware capability and the model will cover a result which 9.8 µm particles separated from the 3.2 µm particles.

5.3 Realistic Comsol Model Results

In this section, the described Comsol model results in 3rd chapter will be demonstrated. The results for 10V electrical potential and 10 µl/min flowrate (0.11 m/s) will be covered in details.

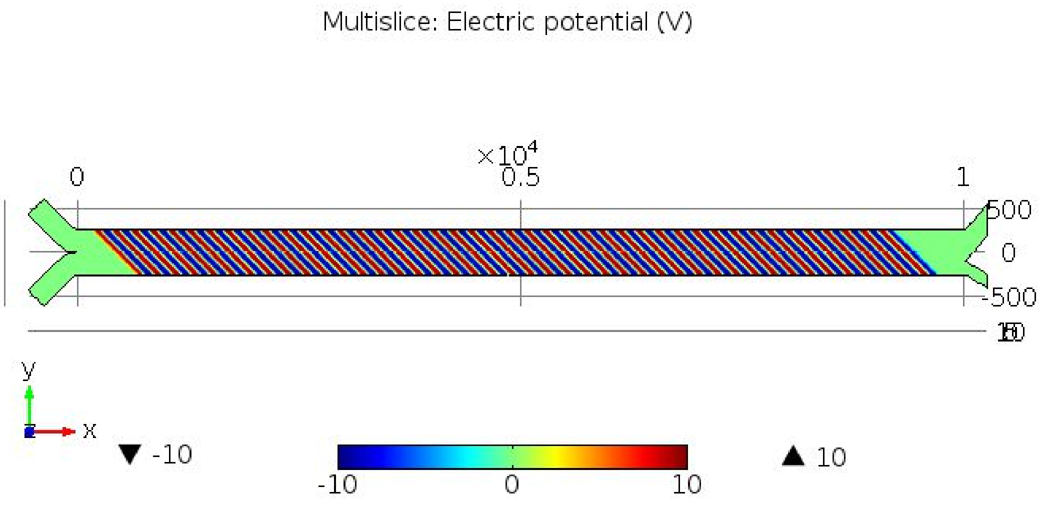

Figure 5.15 : Electric potential of the model

Electric potentials in the model shown in the Figure 5.15 that are coming from -10 V and +10 V load applied to electrode couples. The resulting electric potential distribution along the channel can be seen on Figure 5.16.

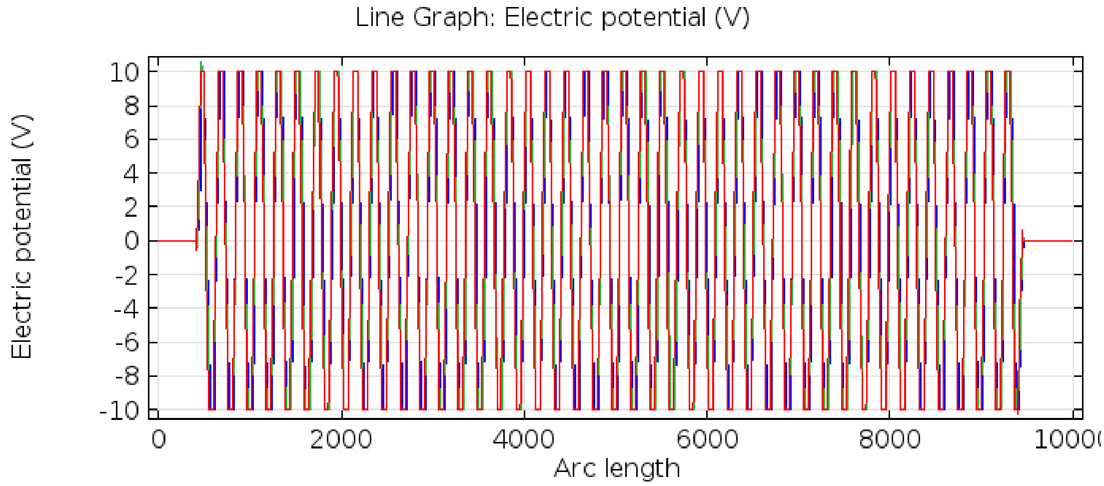

Figure 5.16 : 1D Electrical potential versus the channel length

The resulting electric field of electrical potential shown in Figure 5.16 has been given in Figure 5.17; maximum electric field gradient is around 7x10^5 V m^{-1} and occurs at the edges of the electrodes (Figure 5.18 shows the peaks).

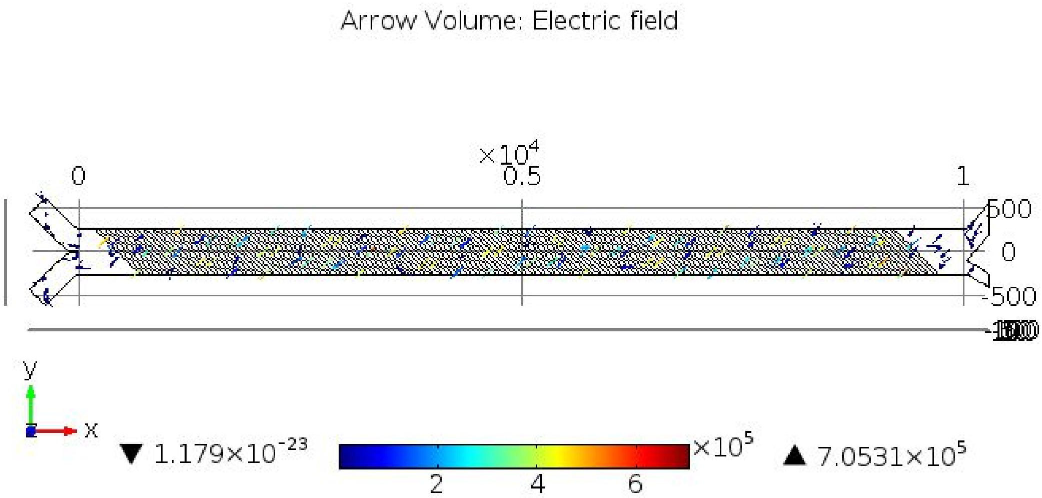

Figure 5.17 : Electrical field of the model

The electrical field shown in Figure 5.18 shows the difference from the simplified model. It creates a periodic DEP force, which results different particle movements than simplified model.

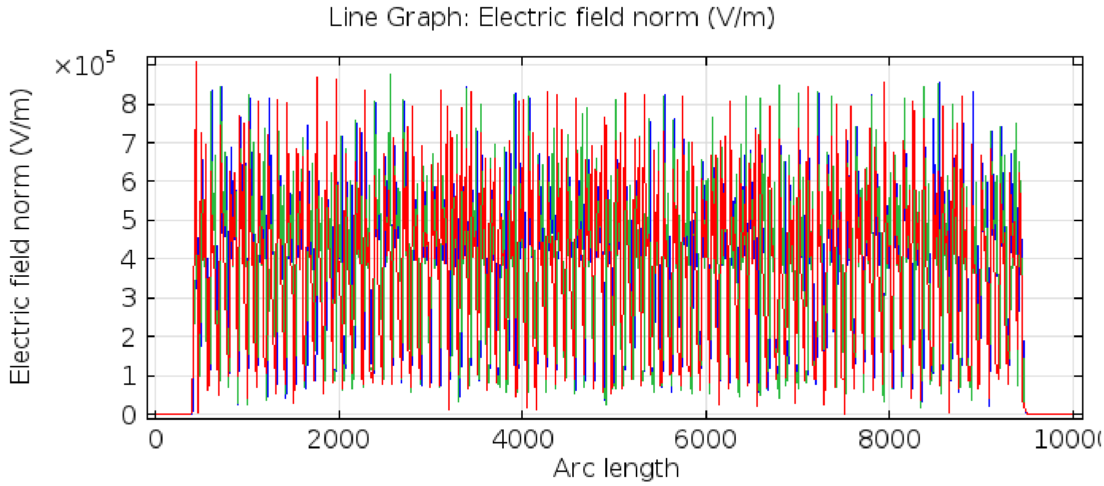

Figure 5.18 : Electrical field distribution along the channel length

Velocity field is shown in Figure 5.19, 0.11 m/s is applied from the two inlets located in the left side. The friction in micro channels neglected and slip boundary condition applied because of that the velocity is very similar near the channel walls; the green profile in Figure 5.20 shows the channel velocity in the center of channel, which is an equal distribution.

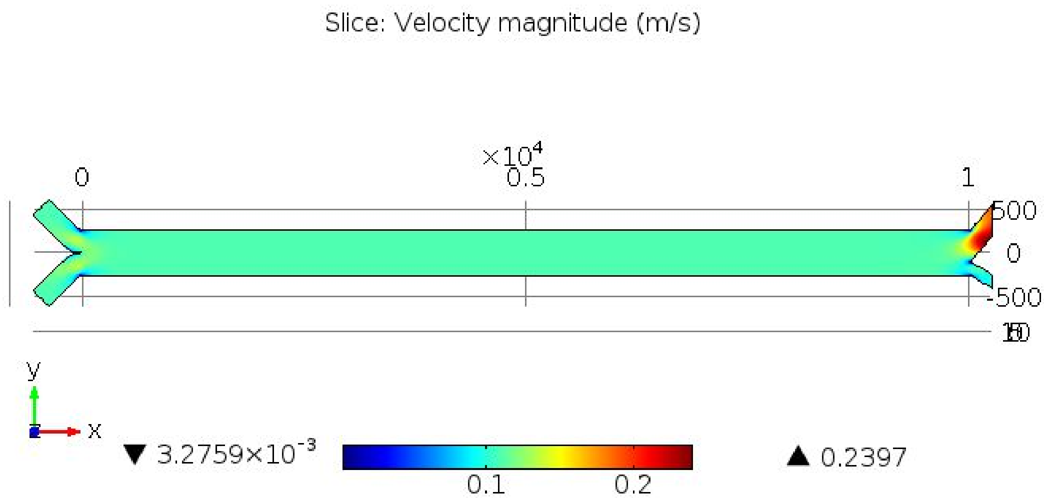

Figure 5.19 : Velocity field of the model

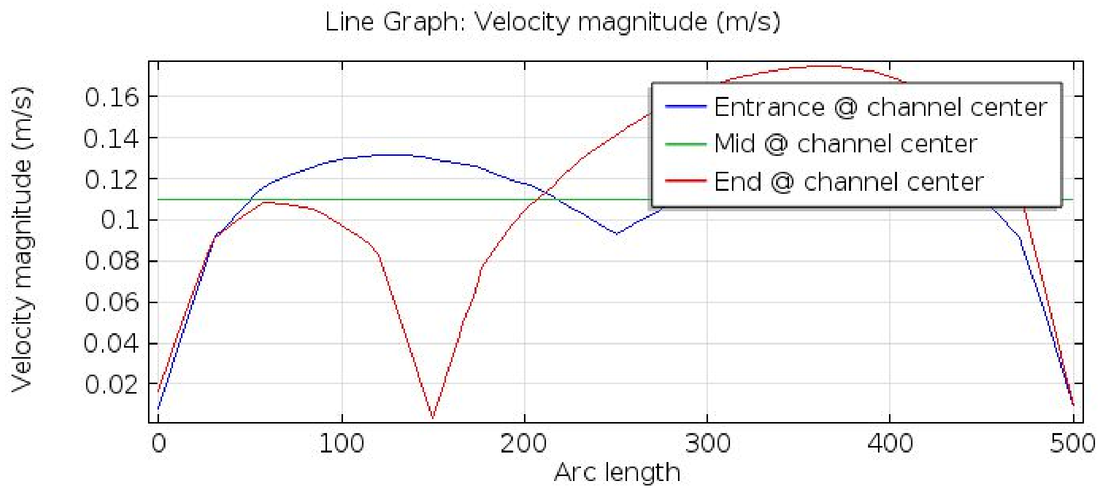

Figure 5.20 : 1D Velocity profile of the channel along the channel width

The generated electric field and velocity field coupled in to the particles and particle flow for fluid flow study performed with time dependently and particle trajectories obtained. In addition, parametric sweep for 3.2 µm: red fluorescent and 9.8 µm: green fluorescent implemented in to the study to solve both in one model and it will enable to obtain single image of both particles' trajectories similar to the simplified model. Figure 5.21 shows the particle trajectories at the end of the simulation. Applied parameters resulted in separation of red and green particles. Red particles leaves the channel from the upper outlet and green ones left from the below outlet.

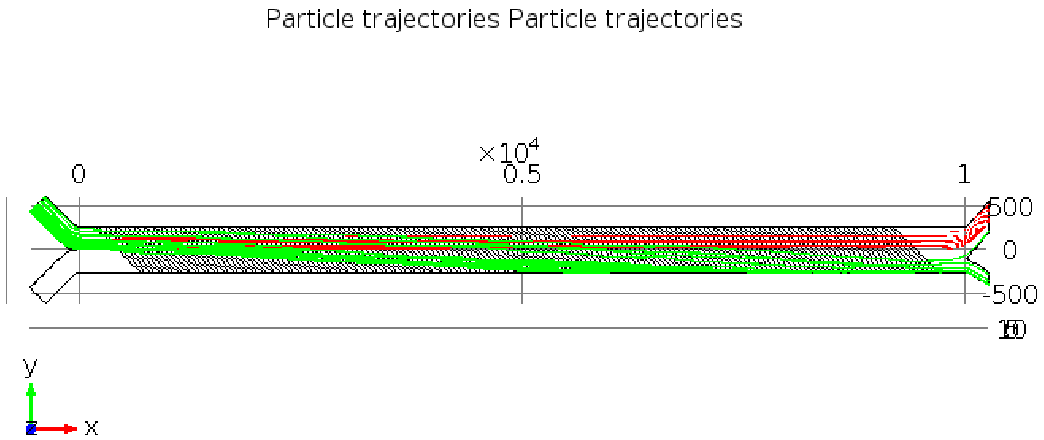

Figure 5.21 : Particle trajectories at 10V potential and 10 µl/min (0.11 m/s)

In order to create a meaningful result separation parameter calculated by using the point average values of all particles. Average of initial position has been subtracted from the final positions and divided by maximum of this position change. Table 5.4 shows the separation percentages of the model according to the particle diameters and average of particle position in initial and final positions.

Table 5.4 : Solution of demonstrated parameters

Flow rate (µl/min)	Velocity (m/s)	Potential Vmax (V)	Particle diameter (µm)	Separation percentage	Start position average (µm)	Final position average (µm)	Change in Point average of particle position in Y axis (µm)
10	0.11	10	3.2	0.115	484	387	97
10	0.11	10	9.8	1.000	484	-363	847

Figure 5.22 shows the particle position average in y direction along the channel and it shows that particles separated.

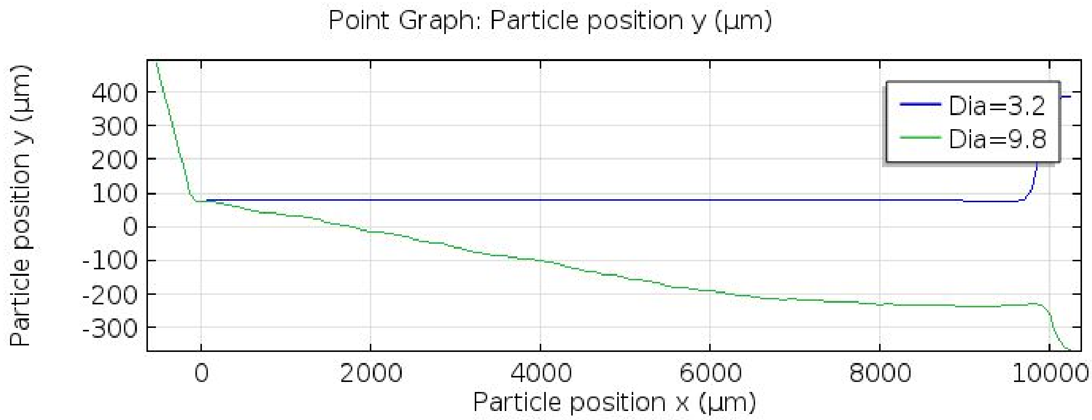

Figure 5.22 : Average particle position changes in Y-axis

In order to understand the reason behind the separation, DEP force Y component on the Figure 5.26 needs to be observed. The effect in 9.8 um particles are much higher and this enables the separation of the larger sized particle.

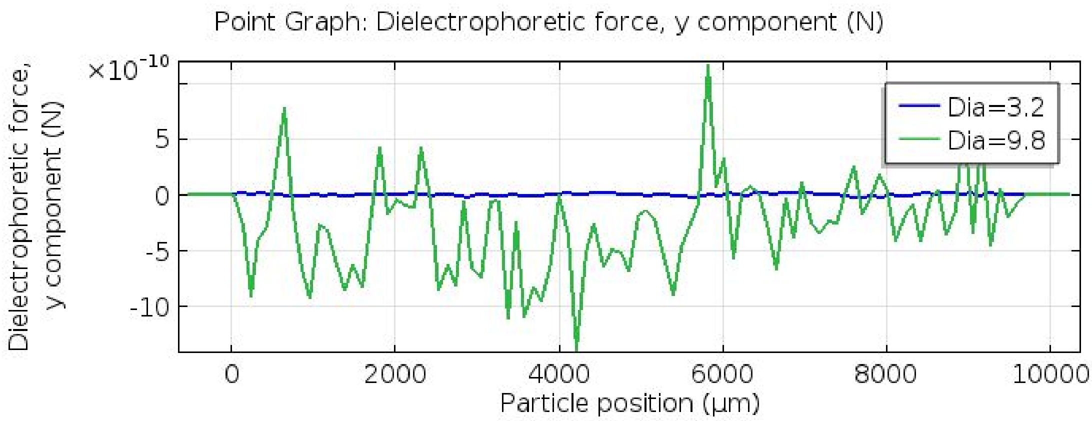

Figure 5.23 : Average DEP force acting on particles at Y-axis

Similar simulations conducted for the different potentials and flow rates and Comsol model characterization completed. The results can be seen in Table 5.5, the green marked rows shows the detailed result demonstrated up to now in this section.

Table 5.5 : Results of the realistic model simulations

Flowrate (µl/dk)	Velocity (m/sn)	Potential Vmax (V)	Particle diameter (µm)	Separation percentage	Start position average (µm)	Final position average (µm)	Change in Y axis (µm)
10	0.11	1	3.2	0.111	484	390	94
10	0.11	1	9.8	0.114	484	388	96
10	0.11	5	3.2	0.110	484	391	94
10	0.11	5	9.8	0.125	484	378	106
10	0.11	10	3.2	0.115	484	387	97
10	0.11	10	9.8	1.000	484	-363	847
20	0.21	1	3.2	0.147	484	359	125
20	0.21	1	9.8	0.124	484	379	105
20	0.21	5	3.2	0.124	484	379	105
20	0.21	5	9.8	0.120	484	382	102
20	0.21	10	3.2	0.102	484	398	87
20	0.21	10	9.8	0.200	484	315	169

The particle trajectories of Table 5.5 (except the 10V potential and 10 µl/min (0.11 m/s) flowrate as it has been shown in details) can be seen at Figure 5.24 to 5.28 and there is no separation observed at any of them.

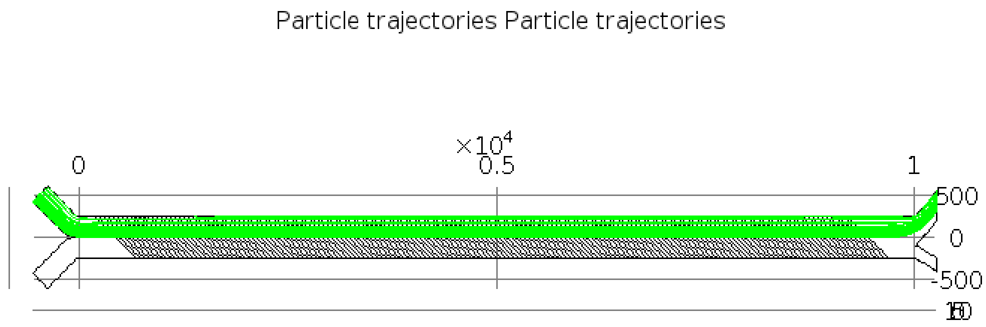

Figure 5.24 : Particle trajectories in 1V potential and 10 μl/min (0.11 m/s) (No separation observed)

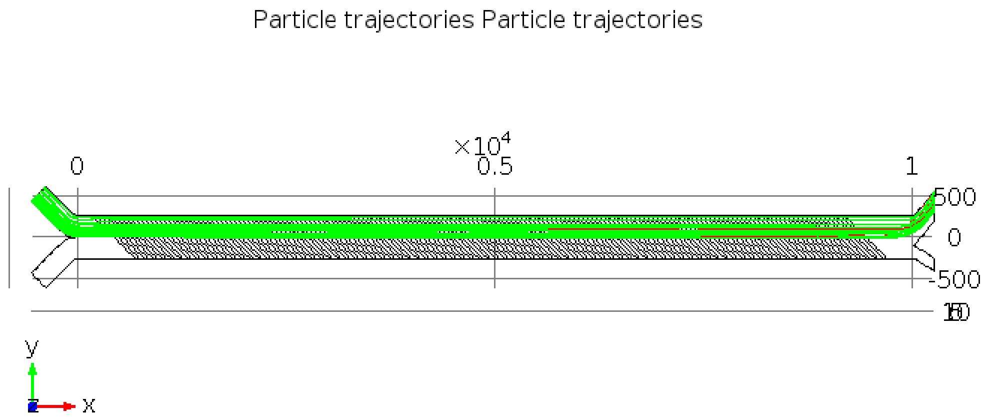

Figure 5.25 : Particle trajectories in 5V potential and 10 μl/min (0.11 m/s) (No separation observed)

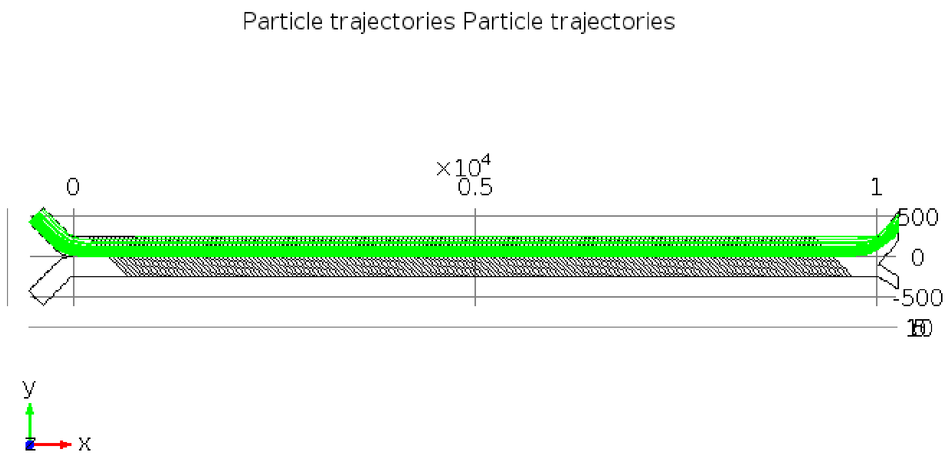

Figure 5.26 : Particle trajectories in 1V potential and 20 μl/min (0.21 m/s) (No separation observed)

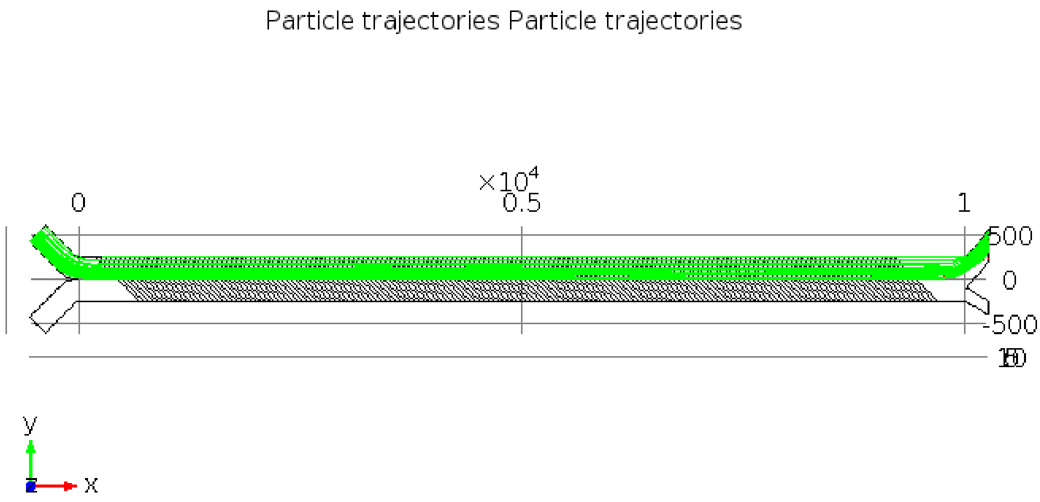

Figure 5.27 : Particle trajectories in 5V potential and 20 µl/min (0.21 m/s) (No separation observed)

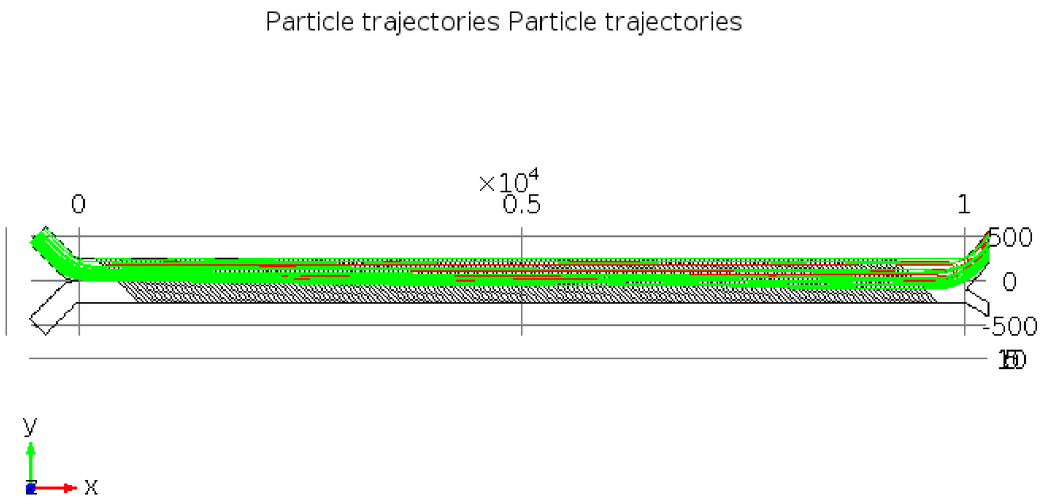

Figure 5.28 : Particle trajectories in 10V potential and 20 µl/min (0.21 m/s) (No separation observed)

In order to compare with the experiments simulation results normalized and explanations are added. They are indicating if the separation occurs or not and summarized in Table 5.6. Only successful separation occurs at the parameters, which are covered in details in this section. In order to compare the results same parameters will be applied at the experiments.

Table 5.6 : Summary of the realistic model simulations

Voltage (V)	Q (µl/min)	Simulation summary		Explanations
		Separation of 3.2 µm	Separation of 9.8 µm	
1	10	0	0	No separation
5	10	0	0	No separation
10	10	0	1	Green particles can be separated from reds
1	20	0	0	No separation
5	20	0	0	No separation
10	20	0	0	No separation

5.4 Experimental Results as A Case Study

Experiment performed in order to compare the Comsol realistic model results, which are demonstrated in the previous chapter. Reference image, region of interest (ROI) has been illustrated in Figure 5.29 and results of the 10 µl/min experiments demonstrated in following Figures from 5.30 to 5.35.

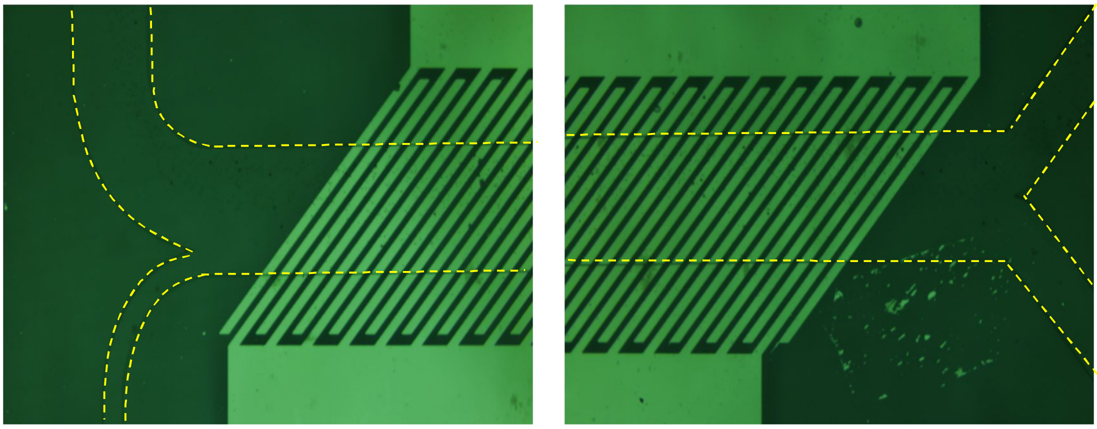

Figure 5.29 : Reference image that shows the region of interest Inlet-Right, Outlet-Left

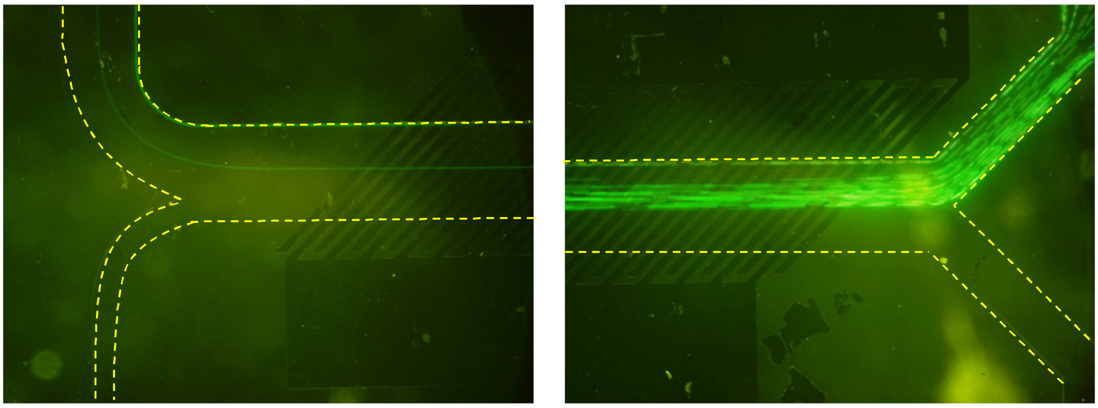

Figure 5.30 : 1V 10 µl/min results that shows green particles are not affected by the negative DEP force

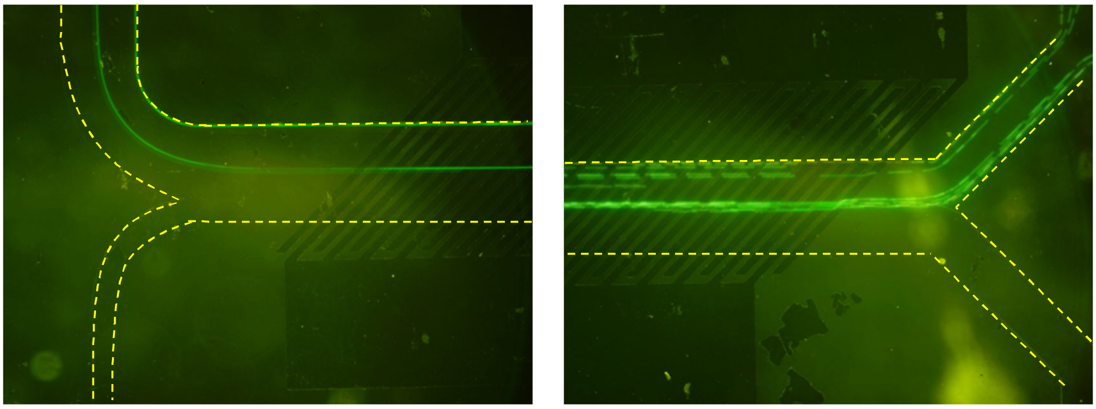

Figure 5.31 : 5V 10 µl/min results that shows green particles are not affected by the negative DEP force

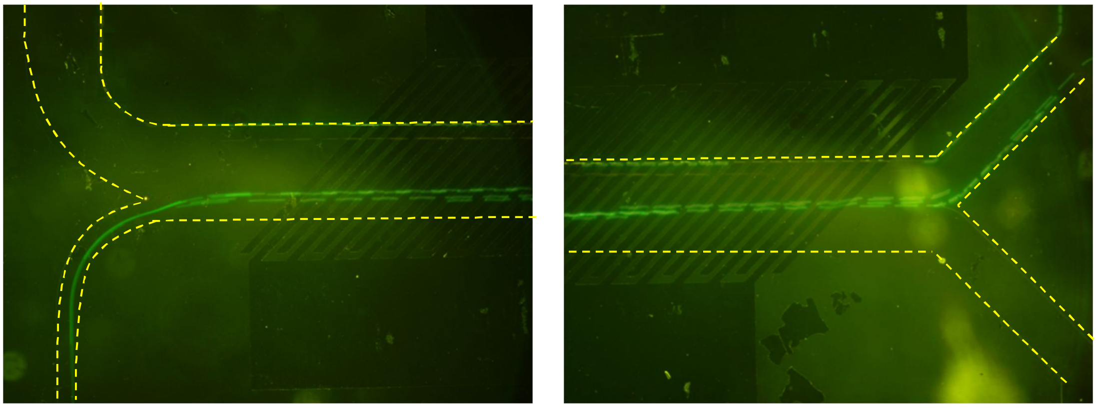

Figure 5.32 : 10V 10 µl/min results that shows green particles are effected by the negative DEP force and leaves the channel from the below outlet

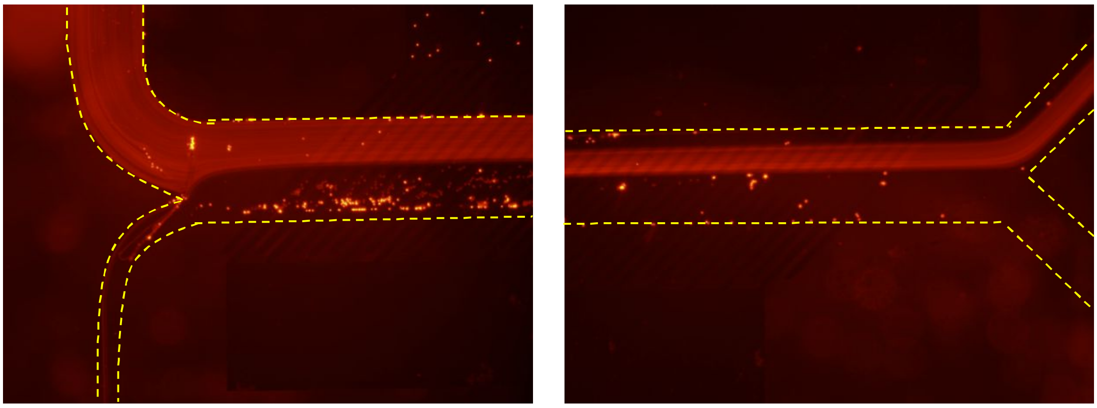

Figure 5.33 : 1V 10 µl/min results that shows red particles are not affected by the negative DEP force

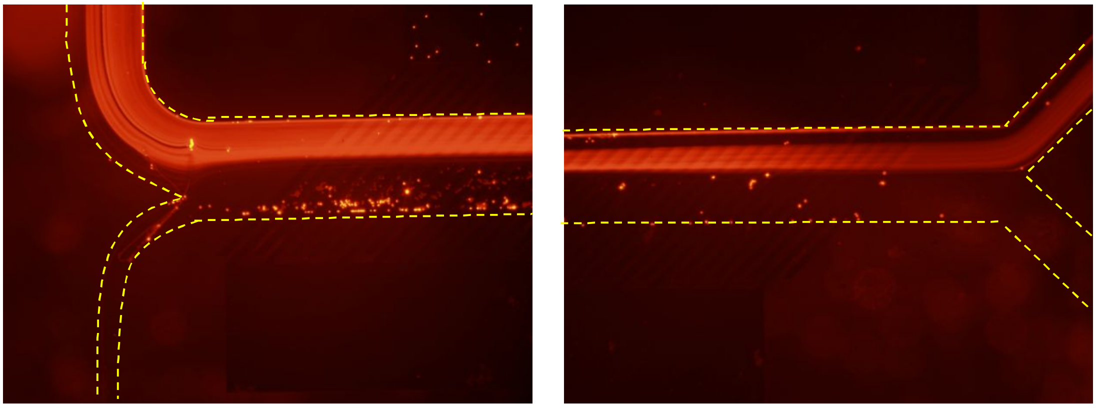

Figure 5.34 : 5V 10 µl/min results that shows red particles are again not effected by the negative DEP force

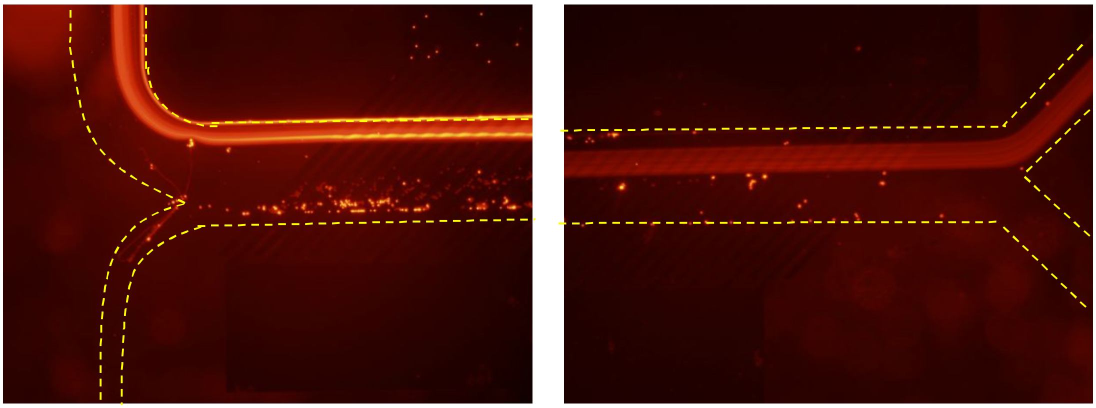

Figure 5.35 : 10V 10 µl/min results that shows green particles are not affected by the negative DEP force

Experimental results of the 20 µl/min is demonstrated from Figure 5.36 to 5.38 as the separation does not occurs at green particles and reds, the results of the red particles are not demonstrated.

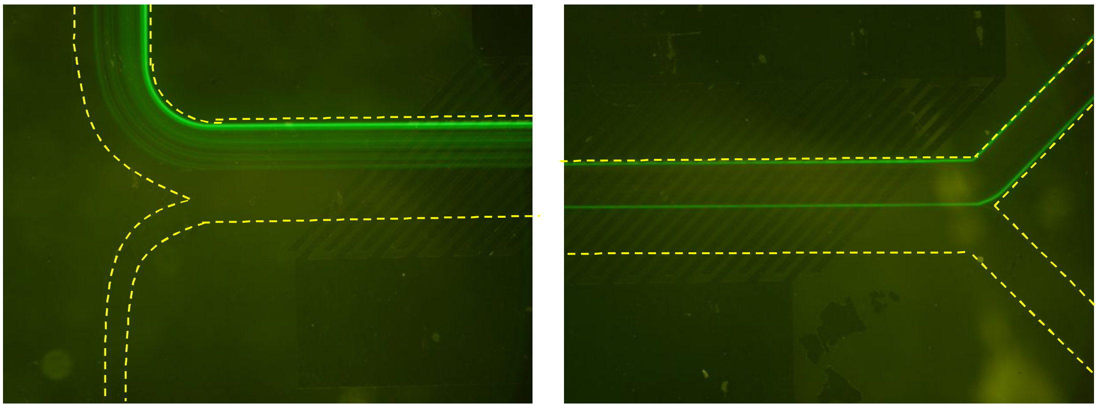

Figure 5.36 : 1V 20 μl/min results that shows green particles are not affected by the negative DEP force

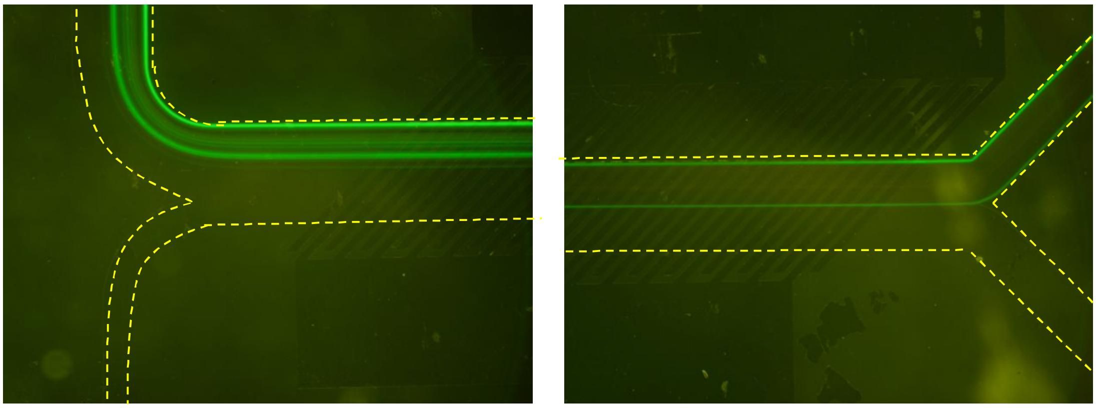

Figure 5.37 : 5V 20 μl/min results that shows green particles are not affected by the negative DEP force

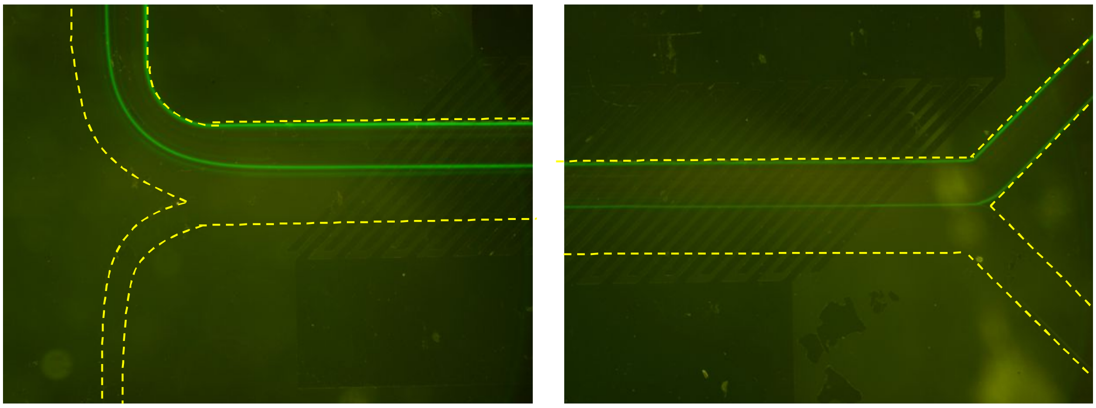

Figure 5.38 : 10V 20 μl/min results that shows green particles are effected by the negative DEP force and leaves the channel from the below outlet

5.5 Comparison of Experimental Results and Simulation Results

Table 5.7 shows the comparison of the results and Figure 5.39 and 5.40 shows the comparison of simulation results and experimental results at 10V potential and 10 μl/min (0.11 m/s) flowrate.

Table 5.7 : Comparison of experiments and simulations

Voltage (V)	Flowrate (μl/min)	V (m/sn)	Simulation summary		Experimental summary		Explanations
			Separation of 3.2 μm	Separation of 9.8 μm	Separation of 3.2 μm	Separation of 9.8 μm	
1	10	0.11	0	0	0	0	No separation
5	10	0.11	0	0	0	0	No separation
10	10	0.11	0	1	0	1	Green particles can be separated from reds
1	20	0.21	0	0	0	0	No separation
5	20	0.21	0	0	0	0	No separation
10	20	0.21	0	0	0	0	No separation

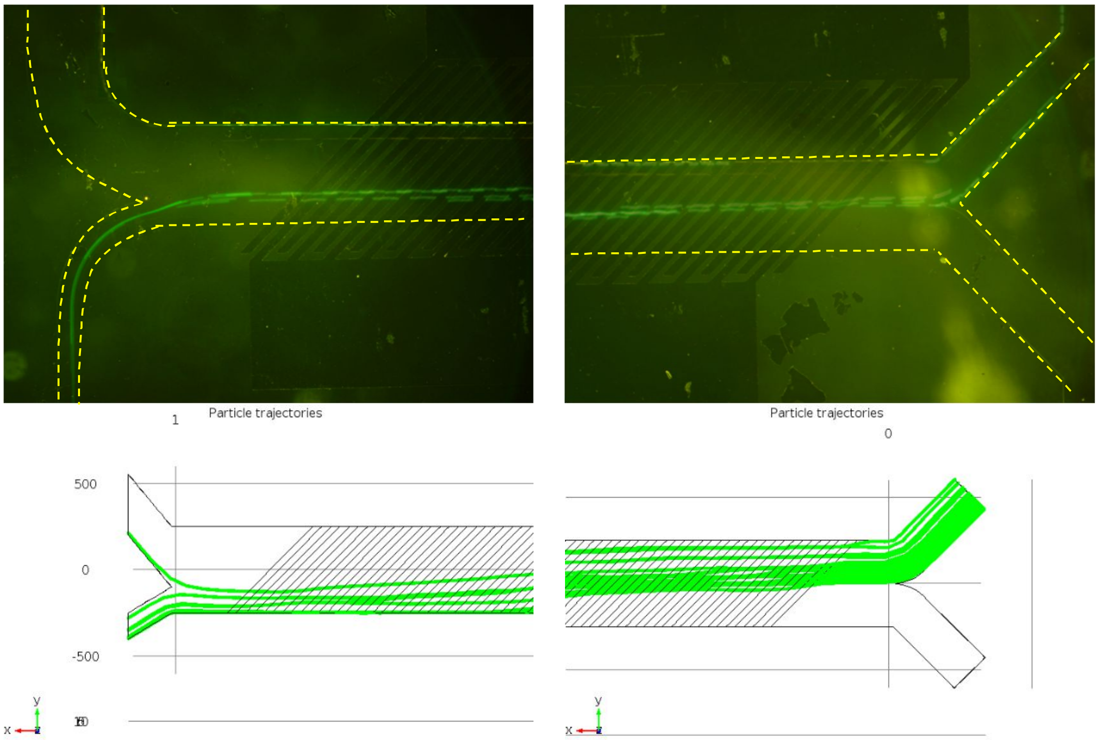

Figure 5.39 : Comparison of 10V 10 μl/min (0.11 m/s) results that shows green particles are effected by the negative DEP force and leaves the channel from the below outlet

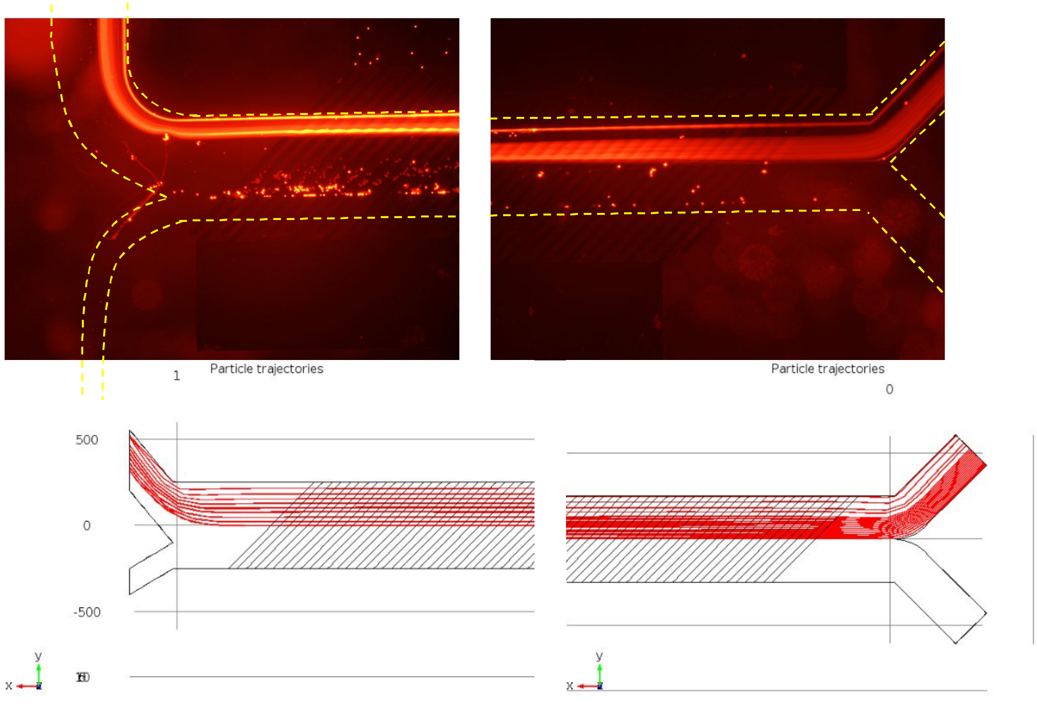

Figure 5.40 : Comparison of 10V 10 µl/min results red particles are not affected by the negative DEP force and leaves the channel from the upper outlet

5.6 Discussion

The below items includes learnings and improvement opportunities for future experimentations and covers some theoretical to experimental relations.

- In order to demonstrate the results better there could be an observation chamber just after the separation point that could be watched under the microscope and where the fluorescence particles can be observed from there and can be compared from the simulation from the same point (Figure 5.41). This will also make characterization easier

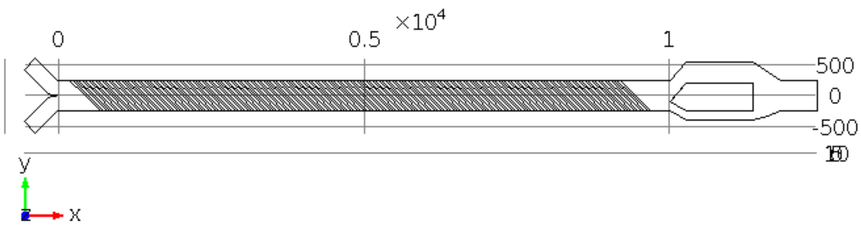

Figure 5.41 : Additional observation chamber

- Electrode angle is also a critical parameter and a more perpendicular electrodes will create a larger DEP force towards the desired channel outlet in y direction and DEP force x component will be less which is opposite to drag force (Figure 5.42)

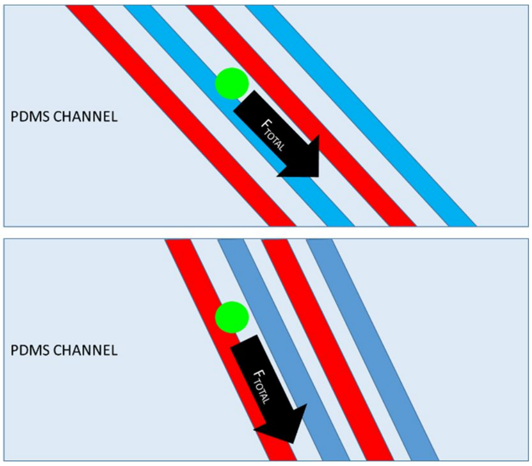

Figure 5.42 : Total acting force to push the particles with more perpendicular electrodes will be higher

- Experiments should always be performed after BSA in PBS solution kept inside the microchannel for 1 day to inhibit fouling, 30 minutes waiting resulted fouling after 1 hour of experimentation
- As a future step, Comsol simulations of living cells can be made with shell models. There is a need to determine the relative permittivity and complex side of the equation should be included in the Comsol model. Simulations should be performed at frequency domain as the cells CM factor includes complex side.
- The simulations also performed at 5 µl/min flowrates but green particles are trapped at 10V potential (Figure 5.43). Similarly, experiments at 5 µl/min resulted trapping of green particles and then they even stucked inside the channel (Figure 5.44). In order not to trap the particles system should run around 10 µl/min flowrates.

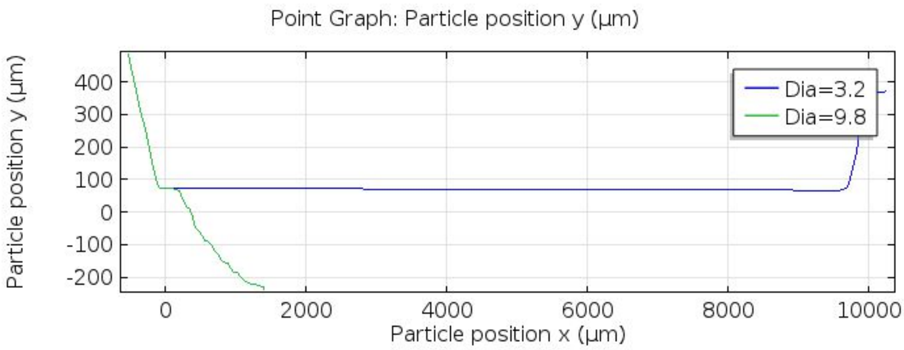

Figure 5.43 : Average particle position changes at y axis (10V and 5 µl/min)

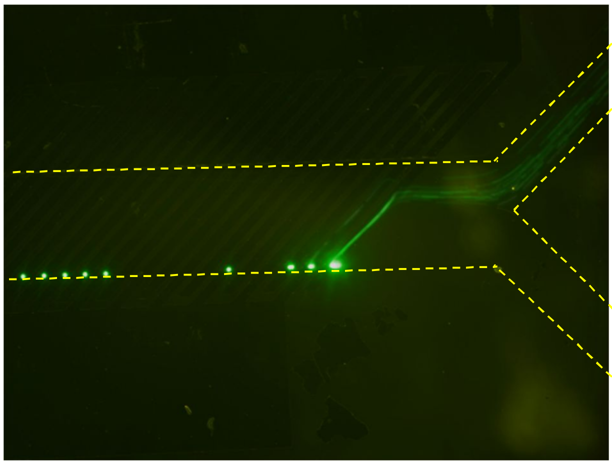

Figure 5.44 : Trapped particles in the inlet of the channel, the experiments performed at 10V and 5 µl/min

6. CONCLUSION

Theoretical background and literature review for the polystyrene particle separation introduced in the first chapter. Design and the simulations of the LOC device explained in the second chapter and a new statistical approach introduced with a simple model. LOC device realistic simulation performed and results introduced in the third chapter. Fabrication of the LOC device and experimental setup explained in details in the fourth chapter. Finally, in the fifth chapter realistic simulation parameters used as experiment condition and results of the experiments shared. As a conclusion, the results introduced in the chapter three matches the results in the fifth chapter and the Comsol simulation of the LOC device is successful. Statistical approach can be used together with the Comsol to help optimization of DEP based LOC devices.

Introduced model can be used to separate biological cells with a known diameter. Comsol simulations can be performed by using the biological cell and medium properties, shell models should be developed for complex side of the cells and mediums relative permittivity and Clausius-Mossotti factor. Super computers can be used to create models that are even more realistic, statistical optimizations can be done prior to experiments, and development times can be reduced by this method.

REFERENCES

Arun, A., Salet, P., & Ionescu, A. M. (2011). Carbon nanotube crossed junction by two step dielectrophoresis. *J Nanosci Nanotechnol, 11*(6), 4919-4922.

Çetin, B. and D. Li (2011). "Dielectrophoresis in microfluidics technology." *ELECTROPHORESIS 32(18)*: 2410-2427.Arun, A., Salet, P., & Ionescu, A. M. (2011). Carbon nanotube crossed junction by two step dielectrophoresis. *J Nanosci Nanotechnol, 11*(6), 4919-4922.

Cetin, B., Kang, Y., Wu, Z., & Li, D. (2009). Continuous particle separation by size via AC-dielectrophoresis using a lab-on-a-chip device with 3-D electrodes. *Electrophoresis, 30*(5), 766-772. doi: 10.1002/elps.200800464

Cornell, J. A. (1987). *Response surfaces: designs and analyses*: Marcel Dekker, Inc.

Du, F., Baune, M., Kück, A., & Thöming, J. (2008). Dielectrophoretic Gold Particle Separation. *Separation Science and Technology, 43*(15), 3842-3855. doi: 10.1080/01496390802365779

Green, N. G., Ramos, A., & Morgan, H. (2002). Numerical solution of the dielectrophoretic and travelling wave forces for interdigitated electrode arrays using the finite element method. *Journal of Electrostatics, 56*(2), 235-254. doi: 10.1016/s0304-3886(02)00069-4

Heller, M. J., Sullivan, B., & Krishnan, R. (2007). DEP system for cancer cell, DNA nanoparticulate and therapeutic nanoparticle detection. *Nanomedicine: Nanotechnology, Biology and Medicine, 3*(4), 337-338. doi: 10.1016/j.nano.2007.10.014

http://www.researchandmarkets.com/. (2011). Biochips Market (DNA Microarrays, Lab-on-Chip, Protein Microarrays, Tissue & Cell Arrays) Trends & Global Forecast (2010-2015). Retrieved 09.11.2014, 2014, from http://www.researchandmarkets.com/research/b1329f/biochips_market_d

http://www.scopus.com/. (2012). from http://www.scopus.com/

Khoshmanesh, K., Nahavandi, S., Baratchi, S., Mitchell, A., & Kalantar-zadeh, K. (2011). Dielectrophoretic platforms for bio-microfluidic systems. *Biosensors and Bioelectronics, 26*(5), 1800-1814. doi: http://dx.doi.org/10.1016/j.bios.2010.09.022

Kim, Y. W., & Yoo, J. Y. (2009). Three-dimensional focusing of red blood cells in microchannel flows for bio-sensing applications. *Biosensors and Bioelectronics, 24*(12), 3677-3682. doi: 10.1016/j.bios.2009.05.037

Lee, H. J., Yasukawa, T., Suzuki, M., Taki, Y., Tanaka, A., Kameyama, M., . . . Matsue, T. (2008). Rapid fabrication of nanoparticles array on polycarbonate membrane based on positive dielectrophoresis. *Sensors and Actuators B: Chemical, 131*(2), 424-431. doi: 10.1016/j.snb.2007.11.051

Li, M., Li, S., Wu, J., Wen, W., Li, W., & Alici, G. (2012). A simple and cost-effective method for fabrication of integrated electronic-microfluidic devices using a laser-patterned PDMS layer. *Microfluidics and Nanofluidics, 12*(5), 751-760. doi: 10.1007/s10404-011-0917-z

Lungu, M., Neculae, A., Bunoiu, M., & Strambeanu, N. (2011). SOME CONSIDERATIONS ON THE NANOPARTICLES MANIPULATION IN FLUID MEDIA USING DIELECTROPHORESIS. *Romanian Journal in Physics, 56*.

Montgomery, D. C. (2013). *Applied Statistics and Probability for Engineers 6th edition*: Wiley.

Nam, S.-W., Kim, S. H., Park, J.-K., & Park, S. (2013). Dielectrophoresis in a Slanted Microchannel for Separation of Microparticles and Bacteria. *J Nanosci Nanotechnol, 13*(12), 7993-7997. doi: 10.1166/jnn.2013.8158

Pethig, R. (2010). Review Article—Dielectrophoresis: Status of the theory, technology, and applications. *Biomicrofluidics, 4*(2).

Salomon, S., Leichlé, T., & Nicu, L. (2011). A dielectrophoretic continuous flow sorter using integrated microelectrodes coupled to a channel constriction. *Electrophoresis, 32*(12), 1508-1514. doi: 10.1002/elps.201000675

Srivastava, S. K., Baylon-Cardiel, J. L., Lapizco-Encinas, B. H., & Minerick, A. R. (2011). A continuous DC-insulator dielectrophoretic sorter of microparticles. *Journal of Chromatography A, 1218*(13), 1780-1789. doi: 10.1016/j.chroma.2011.01.082

Ye, S., & Daniels, K. (2011). *Hierarchical Delaunay triangulation for meshing*. Paper presented at the Proceedings of the 10th international conference on Experimental algorithms, Crete, Greece.

Zhang, C., Khoshmanesh, K., Mitchell, A., & Kalantar-Zadeh, K. (2010). Dielectrophoresis for manipulation of micro/nano particles in microfluidic systems. *Analytical and bioanalytical chemistry, 396*(1), 401-420.

CURRICULUM VITAE

Name Surname: Yavuz GENÇ

Place and Date of Birth: 03 June 1988

Address: Ismetpasa mahallesi, Kızılcam 7 D:22, Kapakli/Tekirdag

E-Mail: gency@itu.edu.tr

B.Sc.: Mechanical Engineering

PUBLICATIONS/PRESENTATIONS ON THE THESIS

- Altınağaç, E., Genç, Y., Sabuncu, A.C., Trabzon, L., Kızıl, H., Beşkök, A. 9th National Conference on Nanoscience and Nanotechnology (NanoTR-9), "Polystyrene Particle Manipulating Using AC Dielectrophoresis", June 24-28, 2013, Erzurum – Turkey.
- Altınağaç, E., Genç, Y., Trabzon, L., Kızıl, H., "Microdevices for Continuous Sized Based Sorting by AC Dielectrophoresis", Micro and Nano Flows 2014, Conference, September, 2014.
- Genç, Y., Altınağaç, E., Trabzon, L., Kızıl, H., Beşkök, A. "Polystren particle separation with Dielectrophoresis", Comsol Conference Cambridge, 2014.
- Genç, Y., Altınağaç, E., Trabzon, L., Kızıl, H. "Simulation and design of a DEP based LOC device for cancer cell separation", Nano-TR Student ITU, 2014, Istanbul – Turkey.
- Altınağaç, E.,Ozcan, S., Genç, Y., Trabzon, L., Kızıl, H. "Biological Particle Manipulation by Dielectrophoresis: An Example of Jurkat Enrichment", NEMS 2015, China